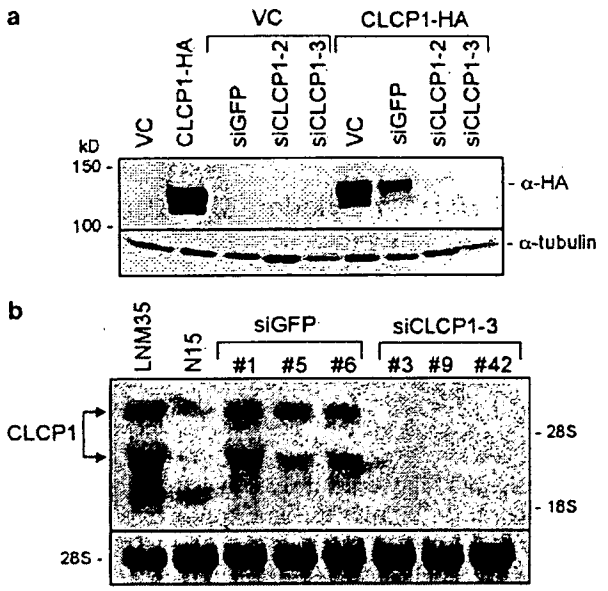

Figure 1 CLCP1 expression and establishment of LNM35-RNAi clones. (a) Immunoblotting of CLCP1-RNAi transfectants. RNAi plasmid vectors were constructed by insertion of the H1 promoter 5′ upstream of the CMV promoter driving a neomycin-resistant gene (pH1-RNA neomycin). CLCP1-RNAi sites were designed at 1196–1214 nt and 1935–1953 nt of *CLCP1* ORFs for siCLCP1–2 and siCLCP1–3, respectively. A blast homology search did not indicate any strong homology for these RNAi sites. 293T cells were transfected with each RNAi-vector along with the HA-tagged CLCP1 expression vector (Koshikawa *et al.*, 2002). A control RNAi construct for the GFP gene, siGFP, was also used. Note the significant reduction of expression of CLCP1 protein observed with siCLCP1–2 and siCLCP1–3. (b) Northern blotting of stable LNM35-RNAi clones. LNM35 was transfected with siCLCP1–3 RNAi constructs and selected with neomycin (1 mg/ml) for 2 weeks. The expression of endogenous *CLCP1* transcripts was almost undetectable in the LNM35 siCLCP1–3 clones (nos. 3, 9 and 42), whereas the high level of expression of *CLCP1* was not affected in control clones that received the siGFP construct. Note the significant difference in *CLCP1* expression level between LNM35 and the parental line N15.

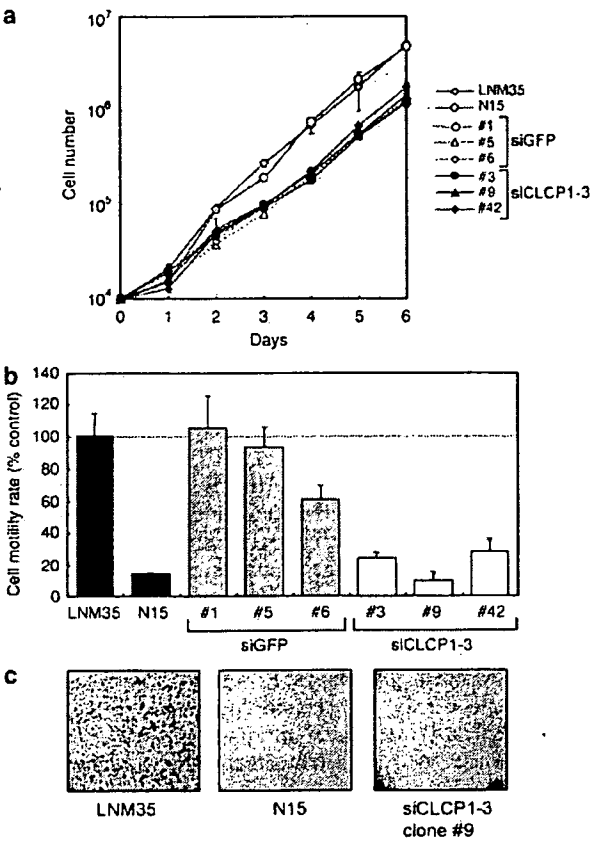

Figure 2 Cell proliferation and motility of LNM35 RNAi clones. (a) Cell proliferation assay. Stable clones were plated at 1×10^4 per dish in RPMI1640 medium with 5% fetal bovine serum and neomycin, then cell numbers were counted each day with a Z1 Coulter Counter (Beckman Coulter, Fullerton, CA, USA). The growth rates of the siCLCP1–3 clones were quite similar to those of the control siGFP clones, (b, c) *in vitro* motility assay. Motility of the RNAi clones was studied using transwell chambers, as described previously (Kozaki *et al.*, 2001) and found to be significantly decreased in all three siCLCP1–3 clones (white bars), whereas the siGFP clones (hatched bars) retained their high levels of motility. (c) A number of migrated cells were observed among the LNM35 cells by Giemsa staining, whereas there were very few N15 or siCLCP1 cells (× 40 magnification). The small dots represent 8 μm-sized transwell chamber pores.

siRNA vector (Figure 1a). To determine whether these findings were associated with decreased cell growth and/or motility of LNM35, we established stable LNM35 transfectant clones. Northern blotting (Figure 1b) revealed that the expression level of *CLCP1* in siCLCP1–3 clones nos. 3, 9 and 42 was significantly reduced to the level of the parental subclone of NCI-H460, N15, whereas *CLCP1* expression was not affected in control siGreen fluorescent protein (siGFP) clones (Supplementary Figure 3). Thereafter, these three siCLCP1–3 clones were employed for further biological analyses.

Cell growth rate was studied and the growth rates of the siCLCP1–3 clones were quite similar to those of siGFP clones (Figure 2a), suggesting that CLCP1 expression is not involved in the regulation of cell growth in LNM35 cells. However, motility was significantly decreased in the siCLCP1–3 clones, whereas the siGFP clones retained high motility (Figure 2b and c), implying that CLCP1 has an effect to enhance cell migration.

Concurrently with the above analyses, we searched for cell surface molecules specific to LNM35 using a phage display method in order to identify the molecular mechanisms of the high motility/invasion ability of LNM35. One of the peptides enriched with this method was SAYIPDS, whose sequence was nearly identical to that of SAYIPES within the SEMA4B gene (Figure 3a). This domain is known to be crucial for interactions with other proteins. CLCP1 has structural similarities to neuropilins, which function as cell surface receptors for semaphorins, therefore, we speculated that the selected peptide and SEMA4B might interact with CLCP1. We compared the interactions of the phage with LNM35 (high CLCP1 expression) and N15 (low CLCP1 expression). When cells were incubated with the phage displaying the

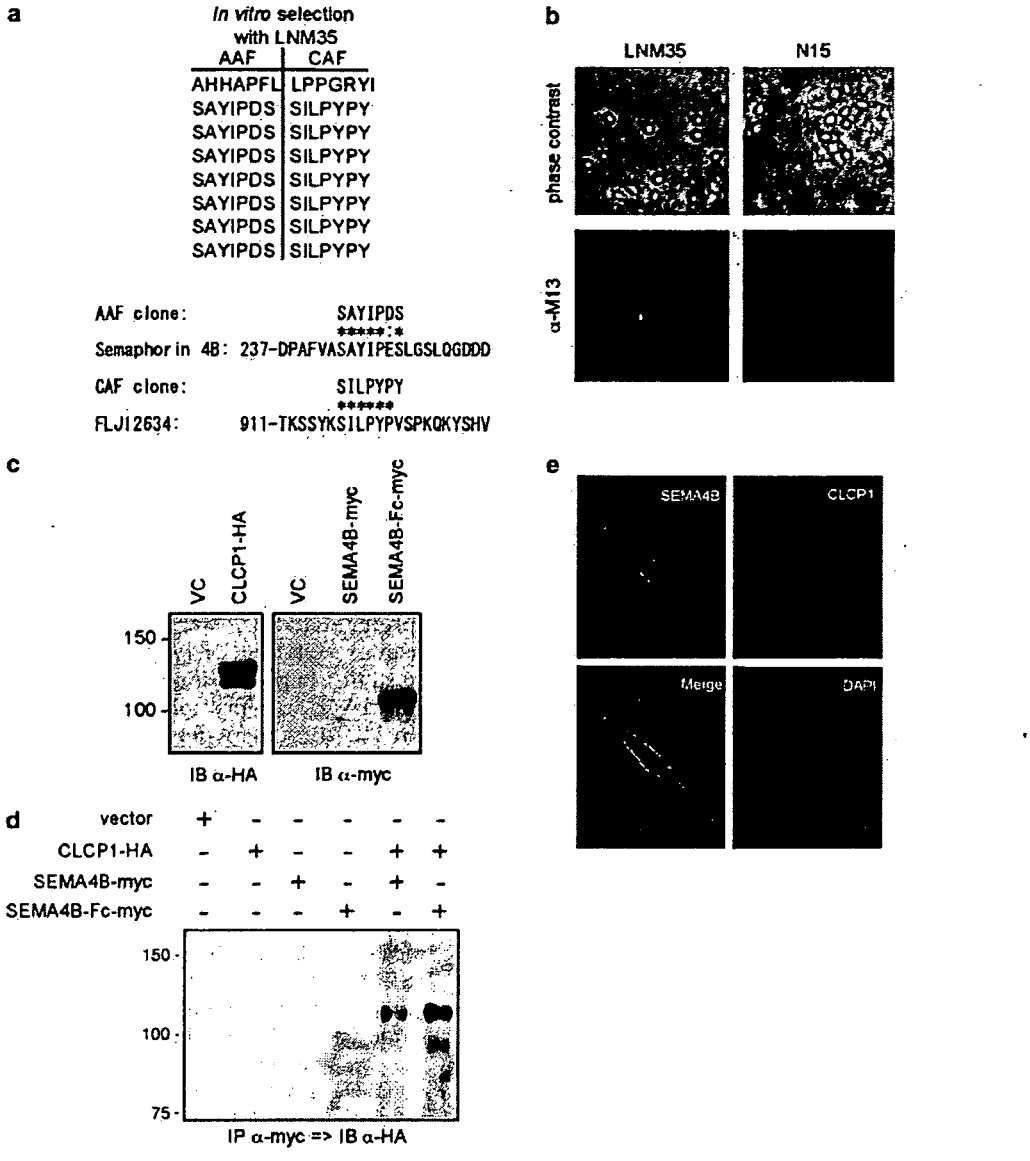

Figure 3 CLCP1 interacts with SEMA4B. (a) *In vitro* selection of LNM35 cells using a phage display library (PhD-7 Phage Display Peptide Library, New England Biolabs, Ipswich, MA, USA). For each selection, $1–2 \times 10^{11}$ PFU of phage particles were overlaid on LNM35 cells. After incubation and washing, attached phages were eluted with acid elution buffer (acid-associated fraction (AAF)). Tightly associated phages were also recovered after cell lysis (cell-associated fraction (CAF)). The phages were amplified following infection with bacteria and rounds of incubation-elution-amplification were repeated. Seven of the eight AAF phage clones sequenced after four rounds of selection contained the SAYIPDS peptide, which was nearly identical to the sequence SAYIPES within the SEMA4B gene. CAF phage results indicated the sequence of a hypothetical protein FLJ12634. (b) Immunofluorescence of phages attached to LNM35. Both LNM35 (with high CLCP1 expression) and N15 (with low CLCP1 expression) cells were incubated with phages displaying the SAYIPDS peptide. After washing and fixation, cell-attached phages were immuno-stained with the monoclonal antibody against M13 procoat protein (GE Healthcare Bio-Science, Piscataway, NJ, USA) and Alexa488-conjugated anti-mouse IgG (Invitrogen, Carlsbad, CA, USA). Note the stronger binding of the SAYIPDS phage with LNM35 as compared to that with N15. (c, d) Co-immunoprecipitation of CLCP1 with SEMA4B. The SEMA4B cDNA clone, KIAA1745, was kindly provided by Kazusa DNA Research Institute. For the SEMA4B-myc expression construct, the SEMA4B ORF was introduced into pcDNA3 (Invitrogen) together with myc-tag at its C-terminus. For the SEMA4B-Fc-myc construct, a 1720-bp *Sac*II-*Bam*HI fragment of KIAA1745 containing only the Sema domain was fused to the cDNA of the human IgG1 Fc portion in the pcDNA vector with an myc-tag at the C-terminus of the Fc portion. SEMA4B-myc or SEMA4B-Fc-myc was co-transfected with CLCP1-HA into 293T cells, and the generated proteins were immunoprecipitated with mouse monoclonal anti-myc-tag antibody 9E10. Immunoblots of these precipitates with rabbit anti-HA antibodies clearly demonstrated co-immunoprecipitation of CLCP1 with SEMA4B proteins. (e) Immunofluorescence of SEMA4B and CLCP1. The A549 lung cancer cell line was transfected with SEMA4B-myc and CLCP1-HA expression vectors, then stained with Alexa Fluor dye-labeled secondary antibodies (Invitrogen) after MG-132 treatment, as performed in Figure 4b and c. Observation with a confocal microscope (Olympus, Tokyo, Japan) showed both CLCP1 and SEMA4B to be mainly localized on the cell surface membrane, with colocalization clearly observed in merged images.

SAYIPDS peptide and then immuno-stained with the anti-M13 antibody against the phage particle, LNM35 staining was more intense than that of N15 (Figure 3b). Next, the indicated interaction between CLCP1 and SEMA4B was studied using an myc-tagged full-length SEMA4B construct, as well as an myc-tagged SEMA4B-Fc fusion construct consisting of the SEMA4B Sema domain and immunoglobulin (Ig)G Fc portion. After co-transfection with hemagglutinin (HA)-CLCP1 into 293T cells, anti-HA immunoblotting of anti-myc immunoprecipitates clearly demonstrated co-precipitation of CLCP1 with SEMA4B or SEMA4B-Fc (Figure 3d). Further, colocalization of CLCP1 and SEMA4B proteins on cell surface membranes was demonstrated by immunofluorescence analysis (Figure 3e).

HA-tagged CLCP1 demonstrated two sizes, 130 and 110 kDa, which were both larger than the predicted molecular mass of 80 kDa. We previously speculated that post-translational modifications such as glycosylation might account for this discrepancy (Koshikawa *et al.*, 2002), as is the case with most transmembrane proteins. To confirm this, 293T cells were transfected with HA-CLCP1 and then treated with tunicamycin, which blocks the first step in the biosynthesis of N-linked oligosaccharides. Tunicamycin treatment reduced the amounts of both the 130- and 110-kDa bands in a dose-dependent manner. Simultaneously, a novel 80-kDa band appeared (Figure 4a), indicating that CLCP1 protein is indeed post-translationally modified by glycosylation, resulting in 130- and 110-kDa-sized proteins, which might be properly processed into transmembrane proteins.

We found that the intensity of the CLCP1 protein band was significantly weaker after CLCP1-SEMA4B co-transfection as compared to with CLCP1 transfection alone (Figure 4b), and subsequently attempted to determine whether SEMA4B caused degradation of CLCP1 protein in a proteasome-dependent manner. When 293T cells were transfected with CLCP1 and/or SEMA4B, and then treated with MG-132, a specific inhibitor of proteasomes, anti-HA immunoblots indicated an increased intensity of both the 130- and 110-kDa bands in the CLCP1 transfectants (Figure 4b, lanes 3 and 4), suggesting that CLCP1 alone was originally regulated by proteasome degradation. However, CLCP1–SEMA4B and CLCP1–SEMA4B-Fc co-transfection were both associated with a significantly reduced intensity of the largest band (130 kDa) (Figure 4b, lanes 5 and 7). Similarly, MG-132 treatment enhanced the intensity of the 110-kDa band (Figure 4b, lanes 4, 6 and 8). However, the 130-kDa band was only moderately restored with CLCP1–SEMA4B co-transfection (Figure 4b, lane 6) and not recovered at all with CLCP1–SEMA4B-Fc co-transfection (Figure 4b, lane 8). In Figure 4c, the size of the co-immunoprecipitated CLCP1 isoform was compared with that of CLCP1 proteins in cell lysates derived from transfectants treated with or without MG-132 or another proteasome inhibitor, lactacystin, which was effective for a Smad4 mutant (Yanagisawa *et al.*, 2000) (Supplementary Figures 1 and 2). The main co-precipitated CLCP1 isoform appeared to be a 110-kDa isoform, even in samples treated with proteasome inhibitors. These findings suggest that the degradation of the 130-kDa band induced by SEMA4B proteins may be too severe to be inhibited by the applied concentration of MG-132. Nevertheless, even with higher concentrations of proteasome inhibitors, full restoration of the 130-kDa band was not obtained (Supplementary Figure 2), suggesting that the interactions with SEMA4B proteins, especially SEMA4B-Fc, may not only induce degradation, but also affect full glycosylation of CLCP1. We also examined the ubiquitination status of CLCP1 using P4D1 monoclonal antibodies that recognize both monoUb and polyUb (Figure 4d). Although ubiquitinated CLCP1 was readily detected in cells co-transfected with the empty vector (Figure 4d, lane 4), the ubiquitination of CLCP1 was significantly increased following co-transfection with SEMA4B (Figure 4d, lane 6). These results suggest that CLCP1–SEMA4B interactions induce significant degradation of CLCP1 proteins, especially 130-kDa fully-glycosylated CLCP1.

This present results indicated that the neuropilin-like protein CLCP1 is upregulated in highly metastatic lung cancer cells and may promote cell motility, possibly resulting in promotion of metastasis. We also found that SEMA4B is a possible ligand of CLCP1, as CLCP1–SEMA4B interaction caused CLCP1 degradation. CLCP1/ESDN was also reported to be expressed by vascular smooth muscle cells, as well as upregulated by platelet-derived growth factor-BB stimulation and vascular injury, suggesting that it modulates growth-promoting signals (Kobuke *et al.*, 2001). Class III semaphorins interact with neuropilins through binding of their Sema and CUB or FV/VIII domains, respectively. Although the interaction domains of CLCP1 and SEMA4B have yet to be determined, it is conceivable that the Sema domain of SEMA4B interacts with CUB and FV/VIII domains of CLCP1. The fact that the sequence within the Sema domain was enriched with the phage display selection in LNM35 expressing CLCP1 provides support for this speculation.

Cell migration is a multistep process that includes leading edge protrusion, focal contact formation and actomyosin-dependent cell contraction, and also involves small guanosine triphosphatase (GTPase) and integrins. Small GTPases, including Rho, Rac and Cdc42, control cell motility by regulating actin and microtubule dynamics (Friedl and Wolf, 2003). Semaphorins and neuropilins make protein complexes with plexins, which regulate the activities of small GTPases through interactions with these small GTPases and Rho-guanine nucleotide exchange factor (Kruger *et al.*, 2005). In addition, a recent report showed that Sema4D-plexin-B1 interaction downregulates R-Ras activity through the endogenous GTPase-activating protein activity of plexin-B1, resulting in inhibition of focal contact mediated by integrins (Oinuma *et al.*, 2004). Therefore, to understand the molecular mechanisms underlying the regulation of cell motility by CLCP1, it is important to clarify whether CLCP1 signaling has any effects on the activities of these small GTPases and integrins.

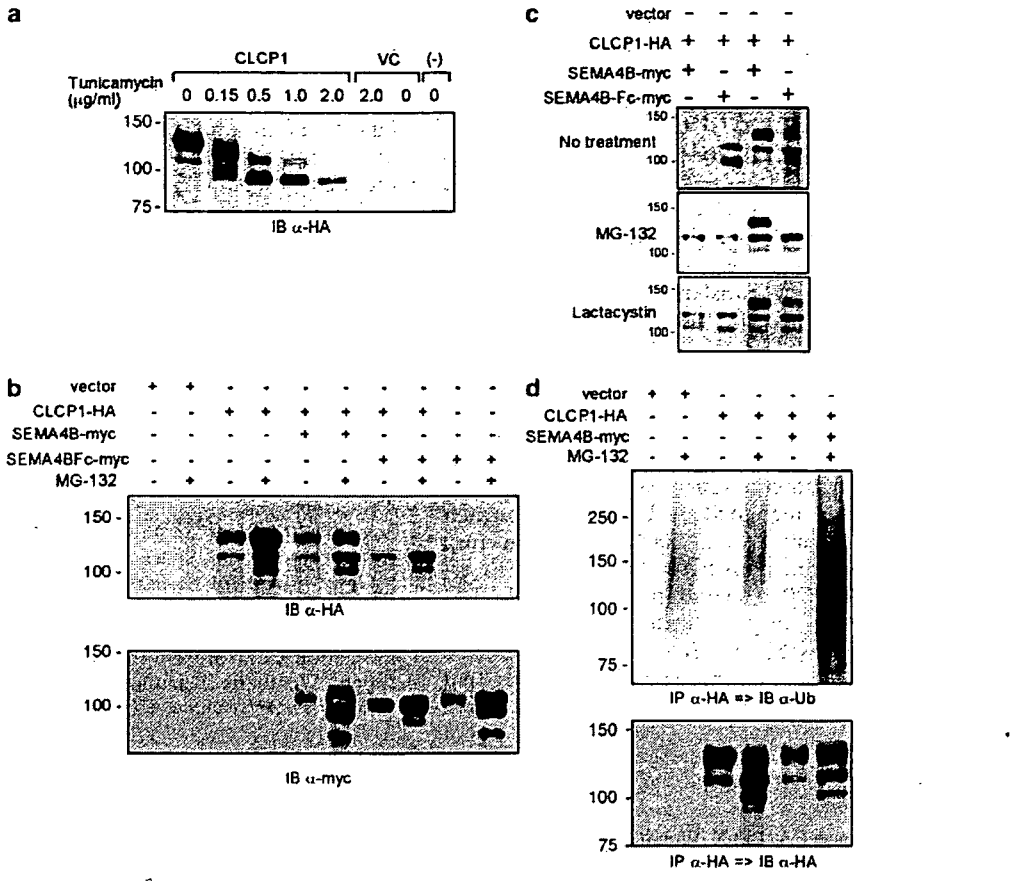

Figure 4 Post-translational modification of CLCP1 protein. (**a**) *N*-glycosylation of CLCP1. 293T cells were transfected with the CLCP1-HA vector and then treated with an *N*-linked glycosylation inhibitor, tunicamycin (Wako Pure Chemical Industries Ltd., Osaka, Japan), for 24 h at the indicated concentrations. Reductions in the amounts of both the 130- and 110-kDa bands resulted, with simultaneous appearance of a novel 90-kDa band similar to the predicted size in a dose-dependent manner. (**b**) Degradation of CLCP1 protein. 293T cells were transfected with CLCP1-HA, SEMA4B-myc and/or SEMA4B-Fc-myc, then treated with a proteasome inhibitor, MG-132 (SIGMA-ALDRICH, St Louis, MO, USA), at 10 μM for 24 h. The expression levels of CLCP1 and SEMA4B proteins were then investigated using anti-HA and anti-myc antibodies. Without MG-132 treatment, the CLCP1 protein band was significantly weaker after CLCP1/SEMA4B or CLCP1/SEMA4B-Fc co-transfection (lanes 5, 7) than with CLCP1 transfection alone (lane 3). MG-132 treatment enhanced the intensity of the CLCP1 protein band in co-transfections (lanes 6, 8) and also with CLCP1 transfection alone (lane 4). Proteasome-dependent degradations of SEMA4B proteins were also observed. (**c**) Analysis of the co-immunoprecipitated isoform of CLCP1. Immunoprecipitation and immunoblotting of CLCP1/SEMA4B and CLCP1/SEMA4B-Fc co-transfected cells were conducted, the same as in Figure 3d. Transfected cells were treated with MG-132 (10 μM) or another proteasome inhibitor, lactacystin (15 μM, Wako Pure Chemical Industries Ltd.). Immunoprecipitated proteins (lane 1, 2) were run with cell lysates before immunoprecipitation (lane 3, 4). The main immunoprecipitated CLCP1 isoform appeared to be the same 110-kDa isoform noted in (**a**). (**d**) Ubiquitination of CLCP1. As in (**b**), 293T cells were transfected and treated with MG-132. Then, CLCP1 protein was immunoprecipitated with the anti-HA antibody and analysed with the anti-ubiquitin antibody, P4D1 (Santa Cruz Biotechnology, Inc., Santa Cruz, CA, USA). Ubiquitination of CLCP1 was readily detected following transfection of CLCP1 alone (lane 4) and significantly increased by co-transfection with SEMA4B (lane 6).

In a previous study, SEMA3A inhibited the migration and spread of a breast cancer cell line, MDA-MB-231, which expresses neuropilin-1 and plexin-A1, whereas another ligand of neuropilin-1, $VEGF_{165}$, was shown to compete with SEMA3A and abrogate its inhibitory effect (Bachelder *et al.*, 2003). CLCP1 may also interact with other ligand molecules, which might regulate cell motility in competition with SEMA4B. In the present study, we also examined the involvement of cyclooxygenase 2 (COX-2) in *CLCP1* expression (Supplementary Figure 4), because a previous study showed that COX-2 was upregulated in LNM35 cells and contributed to their highly metastatic characteristics (Kozaki *et al.*, 2000). We found that nimesulide, a COX-2 inhibitor, repressed *CLCP1* mRNA levels, suggesting a functional association between COX-2 activation and *CLCP1* overexpression in LNM35 cells.

SEMA3B and *SEMA3F*, which are localized at the 3p21.3 locus, are frequently deleted in lung cancers and have been found to suppress tumor cell proliferation (Tse *et al.*, 2002; Xiang *et al.*, 2002; Castro-Rivera *et al.*, 2004). In contrast, class IV semaphorins do not show

such a tumor suppressor function, whereas Sema4D was originally reported to promote B-cell survival and T-cell activation. Another study showed that Sema4D induces angiogenesis, which was mediated by the coupling of its high-affinity receptor plexin-B1 with the Met tyrosine kinase (Conrotto *et al.*, 2005). In addition, class IV semaphorins frequently have PDZ {PSD (postsynaptic density protein) 95, DlgA (Discs large A), and ZO (zonula occludens) 1)} domain-binding motifs at their C-termini, through which they may function as receptors by mediating signal transfers through their intracellular domains. SEMA4B, 4C and 4F have been shown to interact with the PDZ domains of PSD-95 (Inagaki *et al.*, 2001; Burkhardt *et al.*, 2005), whereas SEMA4D was found to associate with CD45 protein tyrosine phosphatase (Herold *et al.*, 1996). Therefore, SEMA4B might function as a CLCP1 receptor. Sema3A–neuropilin interactions induce neuropilin-1 endocytosis, which is mediated by L1-CAM (Fournier *et al.*, 2000; Castellani *et al.*, 2004), which in turn modulates growth cone sensitivity to semaphorin repulsion signals. CLCP1 degradation after CLCP1–SEMA4B interaction may indicate an induction of CLCP1 endocytosis by SEMA4B.

In conclusion, the present results indicate that CLCP1 and its interactions with ligands including SEMA4B may become molecular targets for therapeutic inhibition of metastasis. In addition to CLCP1-siRNA, the suppression of CLCP1 functions with dominant-negative CLCP1 or negatively regulating ligands might inhibit *in vitro* motility and, consequently, *in vivo* metastasis of cancer cells. Fine mapping of the interacting regions between CLCP1 and SEMA4B may indicate concrete molecular targets. Although a full understanding of the biological roles of CLCP1 and SEMA4B remains to be achieved, further investigations of CLCP1 functions should provide novel and useful strategies to improve the clinical prognosis of lung cancer patients by facilitating the suppression of metastasis.

Acknowledgements

This work was supported in part by a Grant-in-Aid for Scientific Research on Priority Areas from the Ministry of Education, Culture, Sports, Science and Technology of Japan, a Grant-in-Aid for Scientific Research (B) and (C) from the Japan Society for the Promotion of Science, and a Grant-in-Aid for the Second Term Comprehensive Ten-Year Strategy for Cancer Control from the Ministry of Health and Welfare, Japan. We thank Kazusa DNA Research Institute for the SEMA4B cDNA clone, KIAA1745.

References

Bachelder RE, Lipscomb EA, Lin X, Wendt MA, Chadborn NH, Eickholt BJ *et al.* (2003). Competing autocrine pathways involving alternative neuropilin-1 ligands regulate chemotaxis of carcinoma cells. *Cancer Res* **63**: 5230–5233.

Burkhardt C, Muller M, Badde A, Garner CC, Gundelfinger ED, Puschel AW. (2005). Semaphorin 4B interacts with the post-synaptic density protein PSD-95/SAP90 and is recruited to synapses through a C-terminal PDZ-binding motif. *FEBS Lett* **579**: 3821–3828.

Castellani V, Falk J, Rougon G. (2004). Semaphorin3A-induced receptor endocytosis during axon guidance responses is mediated by L1 CAM. *Mol Cell Neurosci* **26**: 89–100.

Castro-Rivera E, Ran S, Thorpe P, Minna JD. (2004). Semaphorin 3B (SEMA3B) induces apoptosis in lung and breast cancer, whereas VEGF165 antagonizes this effect. *Proc Natl Acad Sci USA* **101**: 11432–11437.

Conrotto P, Valdembri D, Corso S, Serini G, Tamagnone L, Comoglio PM *et al.* (2005). Sema4D induces angiogenesis through Met recruitment by Plexin B1. *Blood* **105**: 4321–4329.

Fournier AE, Nakamura F, Kawamoto S, Goshima Y, Kalb RG, Strittmatter SM. (2000). Semaphorin3A enhances endocytosis at sites of receptor-F-actin colocalization during growth cone collapse. *J Cell Biol* **149**: 411–422.

Friedl P, Wolf K. (2003). Tumour-cell invasion and migration: diversity and escape mechanisms. *Nat Rev Cancer* **3**: 362–374.

Herold C, Elhabazi A, Bismuth G, Bensussan A, Boumsell L. (1996). CD100 is associated with CD45 at the surface of human T lymphocytes. Role in T cell homotypic adhesion. *J Immunol* **157**: 5262–5268.

Inagaki S, Ohoka Y, Sugimoto H, Fujioka S, Amazaki M, Kurinami H *et al.* (2001). Sema4c, a transmembrane semaphorin, interacts with a post-synaptic density protein, PSD-95. *J Biol Chem* **276**: 9174–9181.

Kobuke K, Furukawa Y, Sugai M, Tanigaki K, Ohashi N, Matsumori A *et al.* (2001). ESDN, a novel neuropilin-like membrane protein cloned from vascular cells with the longest secretory signal sequence among eukaryotes, is up-regulated after vascular injury. *J Biol Chem* **276**: 34105–34114.

Koshikawa K, Osada H, Kozaki K, Konishi H, Masuda A, Tatematsu Y *et al.* (2002). Significant up-regulation of a novel gene, CLCP1, in a highly metastatic lung cancer subline as well as in lung cancers *in vivo*. *Oncogene* **21**: 2822–2828.

Kozaki K, Koshikawa K, Tatematsu Y, Miyaishi O, Saito H, Hida T *et al.* (2001). Multi-faceted analyses of a highly metastatic human lung cancer cell line NCI-H460-LNM35 suggest mimicry of inflammatory cells in metastasis. *Oncogene* **20**: 4228–4234.

Kozaki K, Miyaishi O, Tsukamoto T, Tatematsu Y, Hida T, Takahashi T *et al.* (2000). Establishment and characterization of a human lung cancer cell line NCI-H460-LNM35 with consistent lymphogenous metastasis via both subcutaneous and orthotopic propagation. *Cancer Res* **60**: 2535–2540.

Kruger RP, Aurandt J, Guan KL. (2005). Semaphorins command cells to move. *Nat Rev Mol Cell Biol* **6**: 789–800.

Oinuma I, Ishikawa Y, Katoh H, Negishi M. (2004). The Semaphorin 4D receptor Plexin-B1 is a GTPase activating protein for R-Ras. *Science* **305**: 862–865.

Osada H, Tatematsu Y, Saito H, Yatabe Y, Mitsudomi T, Takahashi T. (2004). Reduced expression of class II histone deacetylase genes is associated with poor prognosis in lung cancer patients. *Int J Cancer* **112**: 26–32.

Tse C, Xiang RH, Bracht T, Naylor SL. (2002). Human Semaphorin 3B (SEMA3B) located at chromosome 3p21.3 suppresses tumor formation in an adenocarcinoma cell line. *Cancer Res* **62**: 542–546.

Xiang R, Davalos AR, Hensel CH, Zhou XJ, Tse C, Naylor SL. (2002). Semaphorin 3F gene from human 3p21.3 suppresses tumor formation in nude mice. *Cancer Res* **62**: 2637–2643.

Yanagisawa K, Uchida K, Nagatake M, Masuda A, Sugiyama M, Saito T *et al.* (2000). Heterogeneities in the biological and biochemical functions of Smad2 and Smad4 mutants naturally occurring in human lung cancers. *Oncogene* **19**: 2305–2311.

Supplementary Information accompanies the paper on the Oncogene website (http://www.nature.com/onc).

Interventional Pulmonology

Respiration

Respiration 2007;74:304–308
DOI: 10.1159/000093233

Received: May 19, 2005
Accepted after revision: November 29, 2005
Published online: May 5, 2006

Clinical Experience with Autofluorescence Imaging System in Patients with Lung Cancers and Precancerous Lesions

Kiyonobu Ueno[a] Yoko Kusunoki[a] Fumio Imamura[a] Mana Yoshimura[a]
Suguru Yamamoto[a] Junji Uchida[a] Yoshitane Tsukamoto[b]

Departments of [a]Pulmonary Oncology, and [b]Pathology, Osaka Medical Center for Cancer and Cardiovascular Diseases, Osaka, Japan

Key Words
Lung cancer · Autofluorescence endoscopy · Autofluorescence imaging system

Abstract
Background: It is important to detect preinvasive bronchial lesions before they become invasive cancer, because detection of early cancer is expected to lead to a cure. Autofluorescence bronchoscopy is a useful device in the detection of preinvasive and cancerous lesions. Recently, a new autofluorescence bronchoscopic system, autofluorescence imaging (AFI) system, has been developed. ***Objectives:*** We evaluated the efficacy of AFI in the diagnosis of precancerous and cancerous lesions. ***Methods:*** A total of 31 patients underwent both conventional white-light bronchoscopy (WLB) and AFI from January 2002 to September 2004. We evaluated autofluorescence findings using a four-point scale: AFI-I, II, III, and B. The findings in WLB were evaluated on a three-point scale: WLB-I, II, and III. Abnormal areas by WLB and AFI were biopsied for histopathological examinations. ***Results:*** A total of 64 lesions were evaluated. When the AFI-III finding was regarded as positive in AFI and WLB-III as positive in WLB, sensitivity for severe dysplasia or worse was 94.7% with AFI and 73.7% with WLB, respectively. ***Conclusions:*** AFI is an effective system for the detection of precancerous and cancerous lesions.

Introduction

Both the incidence and mortality rate of lung cancer are increasing. In 1998, lung cancer deaths first surpassed deaths from gastric cancer, and became the leading cause of death from cancer in both men and women in Japan. Detection of cancer, especially carcinoma in situ (CIS) and microinvasive carcinoma, has been widely expected to lead to a cure. Endobronchial treatments such as photodynamic therapy and brachytherapy have improved the cure rate of the central type of early-stage lung cancer [1–3]. Before endobronchial treatments became clinically applicable, surgical resection was a standard treatment for this stage of lung cancer. Recently, these treatments are considered to be good alternatives for surgery because they can preserve lung volume. Since it is difficult even for experienced bronchoscopists to identify dysplastic and early-stage carcinomatous lesions including CIS by conventional white-light bronchoscopy (WLB) alone, fluorescence endoscopy has been applied to detect these le-

KARGER
Fax +41 61 306 12 34
E-Mail karger@karger.ch
www.karger.com

0025–7931/07/0743–0304$23.50/0

Accessible online at:
www.karger.com/res

Kiyonobu Ueno, MD, PhD
Department of Pulmonary Oncology
Osaka Medical Center for Cancer and Cardiovascular Diseases
1-3-3 Nakamichi, Higashinari-ku, Osaka 537-8511 (Japan)
Tel. +81 6 6972 1181, Fax +81 6 6971 7636, E-Mail ueno-ki@mc.pref.osaka.jp

sions. The laser-induced fluorescence endoscopy (LIFE) system (Xillix, Vancouver, Canada) is one of the autofluorescence bronchoscopic systems developed by Hung and Lam et al. [4–6]. LIFE has been developed to detect the lesions of dysplasia, CIS, and cancers. Recently, a new autofluorescence bronchoscopic system, autofluorescence imaging (AFI), has been developed by Olympus (Olympus Medical Systems Corp., Tokyo Japan). AFI utilizes a videoscope system, and second-generation AFI is capable of displaying both the images of conventional mode and AFI mode on the same monitor by use of a switch. In AFI mode, a combination image of autofluorescence signal and two independent signals from two restricted wavelengths is displayed. By adding autofluorescence information to high-resolution images by conventional mode, holistic diagnosis of endobronchial lesions is expected to become possible. In this paper, we evaluated the efficacy of AFI in the diagnosis of precancerous and cancerous lesions.

Subjects and Methods

AFI System

A charge-coupled device is equipped with filters that cut excitation light in the optical system of the AFI bronchovideoscope to construct images by a 460–690 nm wavelength. The outer diameter of the distal end of the AFI bronchovideoscope is 6.1 mm. From a light source equipped with a 300 W xenon lamp, three lights are irradiated sequentially in AFI mode – the excitation light (395–445 nm) for taking autofluorescence images, and G′-light (550 nm) and R′-light (610 nm) for taking reflected images (G′-image and R′-image, respectively) [7]. Both autofluorescence (460–690 nm) signals and the reflected signals of G′-light and R′-light are processed in the videoprocessor, and composite images are displayed on the monitor as AFI images. The wavelengths of G′-light and R′-light are determined by the hemoglobin's absorption features. Hemoglobin absorbs a large volume of G′-light wavelength and the areas containing more hemoglobin are displayed dark in the G′-image. Consequently, the blood volume (hemoglobin quantity) in the tracheobronchial mucosa is well reflected in the G′-image. On the other hand, hemoglobin absorbs a lesser quantity of R′-light wavelength, and R′-images can afford a basic intensity of signals from the mucosa independently of blood supply [7]. Allocating autofluorescence images to green, G′-images to red, and R′-images to blue, the combined images are constructed by standardizing the intensities of autofluorescence images and G′-images by that of R′-images. AFI displays a green image for normal epithelium. The abnormalities in AFI are basically classified into two patterns, the area expressing magenta color where red is relatively dominant and the area expressing blue color where blue is relatively dominant. In the first generation, AFI lacked the switch that changed two modes of observation images, conventional and AFI mode. In the second generation, a switch was added allowing for the alternating between two modes.

Subjects

A total of 31 patients with risk factors for central-type early lung cancer, 30 men and 1 woman, underwent AFI in our hospital from January 2002 to September 2004. The reasons patients underwent AFI are classified as follows: 10 patients with positive sputum cytology, 8 patients with symptoms including bloody sputum and cough, 11 patients as monitoring after previously treated lung cancer (photodynamic therapy 6, radiotherapy 1, surgical resection 4), and 2 patients as an examination of thoracic malignancy. The mean age was 69 (range 57–80) years old.

Methods

After informed consent was obtained, both WLB and AFI were performed under local anesthesia. We used bronchoscopes (Olympus BF200 or BF240) as WLB and a AFI device as autofluorescence bronchoscopy. Using the first generation of the AFI system, we performed WLB followed by AFI. In this series, 9 patients were enrolled from January to October in 2002. To avoid the bias by bronchoscopic procedure, we performed AFI followed by WLB when the second generation of the AFI device was used. In this series, 22 patients were enrolled from October 2003 to September 2004.

We evaluated the autofluorescence findings using a four-point scale. These evaluations for lesions were done by two or more bronchoscopists. AFI-I images had normal autofluorescence intensity and were green, AFI-III images had much less autofluorescence intensity than AFI-I and appeared magenta. AFI-II images fell in between AFI-I and AFI-III and appeared pinkish-brown. When increased blue color was observed in a lesion, AFI-B was allocated. However, if the lesion showed AFI-II or III in blue image, AFI-II or III was allocated.

Similarly, the findings in WLB were evaluated on a three-point scale. WLB-I was defined as normal mucosa, WLB-II as slightly abnormal mucosa (changes suggesting mild/moderate dysplasia), and WLB-III as severely abnormal mucosa (changes suggesting severe dysplasia and cancer). All abnormal areas with a scale of II or III or B in AFI, or a scale of II or III in WLB underwent biopsies for histopathological examinations. Some areas showing WLB-I and AFI-I also underwent biopsies as negative control.

Results

The mean cigarette index (packs of cigarettes per day × years at that consumption rate) for the 30 smokers was 56 packs (range 3.5–151 packs) and 1 patient was a nonsmoker. The lesions receiving preceding biopsy, radiation therapy, or photodynamic therapy showed AFI-II or AFI-III in spite of their almost normal histology. The same results were seen in LIFE in our previous study. For this reason, we excluded these lesions from the evaluation. Moreover, acute bronchitis showed as a blue image in a wide extent of bronchial mucosa, and the diagnosis of acute bronchitis was facilitated in WLB. These lesions were also excluded in our study. Therefore, 64 lesions were evaluated: 11 lesions were normal, 7 lesions were benign changes including inflammation, fibrosis and hy-

Autofluorescence Imaging System

perplasia. Of 29 dysplastic lesions, 16 were of mild, 11 were moderate, and 2 were severe. Seventeen lesions were cancer, and 1 of these lesions was CIS. The relationship between the AFI scale and histopathological diagnosis is shown in table 1.

Sensitivity for severe dysplasia and cancer by WLB-III was 73.7% and that by AFI-III was 94.7%. Sensitivity for moderate dysplasia or worse by WLB-III was 53.5% and that by AFI-III was 76.6%. Sensitivity and specificity with AFI and WLB were summarized in table 2. A typical case is shown in figure 1a and b. It is noted that 3 squamous cell carcinomas showed AFI-III and WLB-II, and detected correctly by AFI (fig. 1c, d). Examination time for AFI and WLB was 15 min on average. There were no adverse events in adding AFI in bronchoscopic examination.

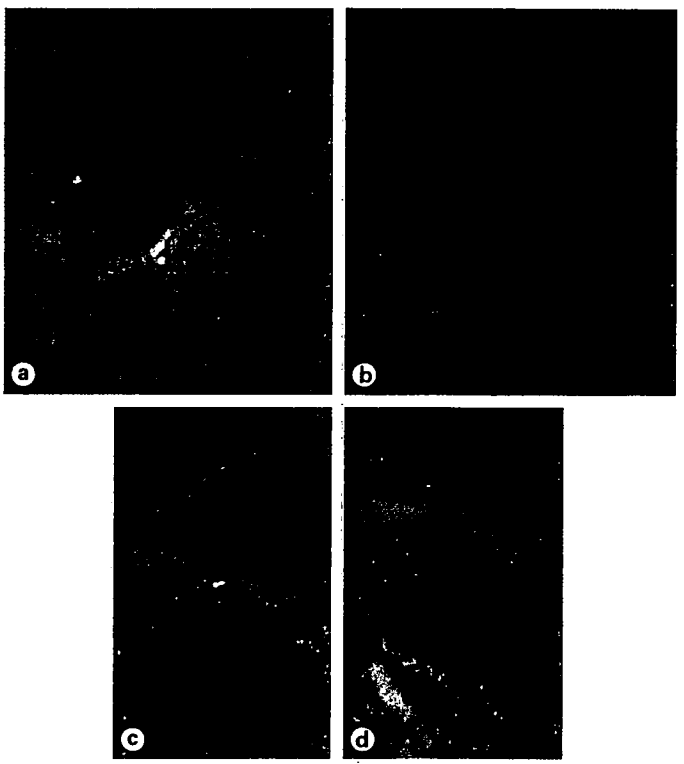

Fig. 1. Squamous cell carcinoma of left B6 (**a** WLB, **b** AFI). Squamous cell carcinoma of right B8+9B10 spur (**c** WLB, **d** AFI).

Table 1. Diagnosis by AFI system and WLB

Histopathology	Biopsy specimens (n = 64)	AFI				WLB		
		AFI-I (n = 19)	AFI-II (n = 11)	AFI-III (n = 31)	AFI-B (n = 3)	WLB-I (n = 17)	WLB-II (n = 17)	WLB-III (n = 18)
Normal + benign changes	18	15	3	0	0	11	7	0
Mild dysplasia	16	2	4	8	2	3	11	2
Moderate dysplasia	11	1	4	5	1	2	7	2
Severe dysplasia	2	1	0	1	0	0	22	0
Cancer	17	0	0	17	0	0	3	14

Table 2. Sensitivity and specificity of AFI and WLB to detect each histopathology

Histopathology	AFI-III		WLB-III	
	sensitivity	specificity	sensitivity	specificity
Moderate dysplasia or worse	76.6%	76.5%	53.3%	94.1%
Severe dysplasia or worse	94.7%	71.1%	73.7%	93.0%
	AFI-II & AFI-III		WLB-II & WLB-III	
	sensitivity	specificity	sensitivity	specificity
Moderate dysplasia or worse	90.0%	50.0%	93.0%	41.2%

Fig. 2. Photomicrograph in the case of AFI-B. Small capillary grows into the moderate dysplastic epithelium. Arrow indicates capillary.

Discussion

Lung cancer is the major cause of cancer death in Japan and most developed countries, and tobacco smoking is one of the causes of this disease. Not only the cessation of smoking, but also early detection and treatment may improve the prognosis of this disease. It is well known that autofluorescence bronchoscopy can improve the detection rate of endobronchial lesions in high-risk groups [8], although Kurie et al. [9] reported that LIFE did not improve the detection of dysplasia or squamous metaplasia. The patient population in Kurie's study may have had a lower possibility of preinvasive cancer than in the other studies.

LIFE, D-light system (Storz, Tuttlingen, Germany), SAFE 1000 autofluorescence system (Pentax, Asahi Optical Tokyo, Japan), and DAFE system (Wolf, Knittlingen, Germany) are commercially available autofluorescence bronchoscopy systems [10–12]. We have been using the LIFE-lung system in clinical practice. LIFE-Lung uses a helium-cadmium laser for excitation at 442 nm, and the emission spectrum is captured by two charge-coupled device cameras and processed through a fluorescence collection sensor and optical multichannel analyzer. Real-time digitized images are acquired by the ratios of red to green (520–630 nm) fluorescence emissions. In comparison, AFI uses a xenon lamp, and lacks a laser generator. AFI afforded clearer images than LIFE because of the utilization of a videoscope system. Moreover, the switch for independent viewing of the two modes of observation reduced the examination time for AFI. In practical use, this switch will be useful because of the need for repeated observations of suspicious areas.

We found the sensitivity of AFI in detection of severe dysplasia and cancer was 94.7%, and the sensitivity of AFI was 21.0% higher than that of WLB. We previously reported that sensitivity of LIFE for detection of severe dysplasia or worse was 83.7% [13]. Sensitivity of LIFE for detection of moderate dysplasia or worse is reported in other literature to lie between 38.0 and 91.0% [14]. In this study, the sensitivity of AFI for detection of moderate or worse was 76.6%. In our study, 3 squamous cell carcinomas diagnosed as moderate dysplasia (WLB-II) in WLB and cancer (AFI-III) in AFI. Haussinger et al. [15] reported that detection of CIS is not increased by autofluorescence bronchoscopy. The reasons for this discrepancy are as follows: sample size of our study was small, and we used a four-point scale in AFI and a three-point scale in WLB, but Haussinger et al. used a two-point scale. Indeed, these lesions were abnormal in both AFI and WLB if we used a two-point scale.

If only WLB-III in WLB is judged as abnormal without considering the AFI finding, 4 lesions with severe dysplasia or worse are missed. These results suggested that AFI has comparable diagnostic ability for detecting precancerous lesion to the other autofluorescence bronchoscopic systems such as LIFE.

Recently, Chiyo et al. [7] compared prospectively AFI with WLB and LIFE. Sensitivity and specificity of AFI for mild, moderate, and severe dysplasia was 80 and 83.3%, respectively. They excluded 2 squamous cell carcinomas which could be detected by all 3 modalities from their analysis; AFI-II and AFI-III in our criteria were judged to be positive in their analysis. In the analysis of our data on the same condition as theirs, sensitivity and specificity were 76.7% (23/30) and 83.0% (15/18), respectively. These results were almost comparable with theirs.

Sensitivity and specificity of the first generation of AFI were not significantly different from those of the second (data not shown). This means that the diagnostic ability of AFI is not dependent upon the order of bronchoscopic procedure. Hirsch et al.'s [14] report also showed that there was no difference in the sensitivity and specificity, regardless of the order of the bronchoscopic procedure.

Tracheobronchial mucosa that contains a large amount of blood should be indicated by blue images with AFI. The extended vessels in mucosa and any bleeding area are actually shown in blue. Most of the lesions that exhibited blue in AFI were inflammation unless they were bleeding. However, three blue lesions in AFI were mild or moderate dysplasias (fig. 2). The reason for this is not clear at present. Angiogenic squamous dysplasia (ASD) is a newly recognized morphological entity. ASD consists of capillary blood vessels closely juxtaposed to and pro-

jected into metaplastic or dysplastic squamous epithelium [16]. Keith et al. [16] reported that ASD was observed in many high-risk smokers and patients with squamous cell cancer and may represent an important intermediate pathological biomarker preceding lung cancer development. Two of three blue lesions showed an increased number of microcapillaries and this might result in increasing blood supply in the mucosa; an increase in the blood supply results in an increase in the blue signal. LIFE detected more ASD lesions than WLB. Regarding hemoglobin content, AFI has more information than LIFE because of adding R'-image information. AFI may be useful for detecting ASD.

We conclude that AFI is a useful system to detect cancer and precancerous lesions, and is used for screening of the high-risk group. Since the number of severe dysplasias and CIS was small in our study, multicenter trials will be necessary to confirm this conclusion.

Acknowledgement

We thank Olympus Medical Systems Corp. Ltd for technical support for the AFI system.

References

1 Furuse K, Fukuoka M, Kato H, Horai T, Kubota K, Kodama N, Kusunoki Y, Takifuji N, Okunaka T, Konaka C, Wada H, Hayata Y: A prospective phase II study on photodynamic therapy with photofrin II for centrally located early-stage lung cancer. J Clin Oncol 1993;11: 1852–1857.

2 Sutedja TG, Postmus PE: Photodynamic therapy in lung cancer: a review. J Photochem Photobiol B 1996;36:199–204.

3 Speiser BL: Strategies for treatment of occult carcinomas of the endobronchus. Chest 1997; 111:1158–1161.

4 Hung J, Lam S, LeRiche JC, Palcic B: Autofluorescence of normal and malignant bronchial tissue. Laser Surg Med 1991;11:99–105.

5 Lam S, MacAulay C, Hung J, LeRieche J, Profio AE, Palcic B: Detection of dysplasia and carcinoma in situ with a lung imaging fluorescence endoscope device. J Thorac Cardiovasc Surg 1993;105:1035–1040.

6 Lam S, MacAulay C, LeRiche JC, Ikeda N, Palcic B: Early localization of bronchogenic carcinoma. Diagn Ther Endosc 1994;1:75–78.

7 Chiyo M, Shibuya K, Hoshino H, Yasufuku K, Sekine Y, Iizawa T, Hiroshima K, Fujisawa T: Effective detection of bronchial preinvasive lesions by a new autofluorescence imaging bronchovideoscope system. Lung Cancer 2005;48: 307–317.

8 Sutedja TG, Venmans BJ, Smit EF, Postmus PE: Fluorescence bronchoscopy for early detection of lung cancer: a clinical perspective. Lung Cancer 2001;34:157–168.

9 Kurie JM, Lee JS, Morice RC, Walsh GL, Khuri FR, Broxson A, Ro JY, Franklin WA, Yu R, Hong WK: Autofluorescence bronchoscopy in the detection of squamous metaplasia and dysplasia in current and former smokers. J Natl Cancer Inst 1998;90:991–995.

10 Haussinger K, Pichler J, Stanzel F, Markus A, Stepp H, Morresi-Hauff A, Baumgartner R: Autofluorescence bronchoscopy; the D-light system. Progr Respir Res 2000;30:243–252.

11 Kakihana M, Kim KI, Okunaka T, Furukawa K, Hirano T, Konaka T, Kato H, Ebihara Y: Early detection of bronchial lesions using system of autofluorescence endoscopy (SAFE) 1000. Diagn Ther Endosc 1999;5:99–104.

12 Herth FJ, Ernst A, Becker HD: Autofluorescence bronchoscopy – a comparison of two systems (LIFE and D-light). Respiration 2003;70: 395–398.

13 Kusunoki Y, Imamura F, Uda H, Mano M, Horai T: Early detection of lung cancer with laser-induced fluorescence endoscopy and spectrofluorometry. Chest 2000;118:1776–1782.

14 Hirsch FR, Prindiville SA, Miller YE, Franklin WA, Dempsey EC, Murphy JR, Bunn PA Jr, Kennedy TC: Fluorescence versus white-light bronchoscopy for detection of preneoplastic lesion: a randomized study. J Natl Cancer Inst 2001;93:1385–1391.

15 Haussinger K, Becker H, Stanzel F, Kreuzer A, Schmidt B, Strausz J, Caveliere S, Herth F, Kohlhaufl M, Muller KM, Huber RM, Pichlmeier U, Bolliger CT: Autofluorescence bronchoscopy with white light bronchoscopy alone for the detection of precancerous lesions: a European randomized controlled multicentre trial. Thorax 2005;60: 496–503.

16 Keith RL, Miller YE, Gemmill RM, Drabkin HA, Dempsey EC, Kennedy TC, Prindiville S, Franklin WA: Angiogenic squamous dysplasia in bronchi of individuals at high risk for lung cancer. Clin Cancer Res 2000;6:1611–1625.

Pathology International 2007; 57: 229–231 doi:10.1111/j.1440-1827.2007.02086.x

Letter to the Editor

Pleural sarcomatoid malignant mesothelioma consisting of histiocytoid cells

To the Editor:

Pleural sarcomatoid malignant mesothelioma (PSMM) consists of spindle cells arranged in fascicles or having a haphazard fashion. The pattern often resembles fibrosarcoma, but marked anaplasia and bizarre multinucleated tumor cells may result in a picture closely mimicking that of malignant fibrous histiocytoma.[1] We herein report an extremely rare case of PSMM consisting of histiocytoid cells without any inflammatory infiltrate. We discuss its differential diagnosis and the key to establishing an accurate diagnosis.

A 76-year-old Japanese woman, a non-smoker, consulted Osaka Prefectural Medical Center for Respiratory and Allergic Diseases complaining of left chest pain that had persisted for the previous 2 weeks. She had worked as a spinning-mill worker for more than 30 years and occupational exposure to asbestos was highly supported. She had a past history of pleuritis and pericarditis of unknown origin. Chest X-ray demonstrated two fist-sized subpleural nodules in the left mediastinal and parietal costal pleura without any pulmonary lesions. There was a large amount of bloody pleural effusion on the left side. Pleural effusion cytology did not demonstrate any neoplastic findings. The course of the disease was rapidly progressive. A tentative clinical diagnosis of pleuritis carcinomatosa was made and percutaneous needle biopsies were obtained from the subpleural lesions. Histologically, most tumor cells infiltrated into a myxoid stroma and grew as a diffuse pattern (Fig. 1a). Sheets and nests of cells were absent. Inflammatory infiltrate was slight. The tumor cells were mainly composed of histiocytoid cells (Fig. 1b). These histiocytoid cells were ovoid or polyhedral in shape, with palely eosinophilic or foamy cytoplasm. Their nuclei were medium to large, ovoid or angulated, contained fine chromatin, and inconspicuous nucleoli (Fig. 1c). Multinucleated giant tumor cells were rarely recognized. Mitoses were 2/10 high-power fields (HPF). Necrosis and hemorrhagic areas were absent. Reactive histiocytes were sometimes present among these neoplastic cells. Immunohistochemical studies showed that these tumor cells were positive for AE1/AE3 (Fig. 2a), D2-40 (Fig. 2b), HBME-1, vimentin and WT-1 (Fig. 2c), but negative for BerEP4, CA125, calretinin, CAM5.2, CD3, CD15, CD30, CD34, CD45RB, CD79α, CEA, cytokeratin 5/6, cytokeratin 7, desmin, epithelial membrane antigen, napsin A, PE-10, PG-M1, S-100, Smooth-muscle actin, thrombomodulin and thyroid transcription factor-1. MIB-1 was positive in 20% of tumor cells. PAS reaction was positive in some tumor cells and was partly digested with diastase. Alcian blue stain was positive in stroma digested with hyaluronidase and negative in the cytoplasm. Colloidal iron stain was positive in the stroma and digested with hyaluronidase. Taken together, we made a diagnosis of pleural sarcomatoid malignant mesothelioma consisting of histiocytoid cells.

Recognition of this rare variant of malignant mesothelioma is important because of the possibility of confusing it with lymphohistiocytic variant of anaplastic large cell lymphoma (LHALCL), sarcomatoid carcinoma (SC) of the lung or thymus, inflammatory malignant fibrous histiocytoma (IMFH), inflammatory myofibroblastic tumor (IMT) or lymphohistiocytoid mesothelioma (LHM). In LHALCL, large-sized atypical cells with immunohistochemical CD30 positivity are admixed with histiocytes and plasma cells.[2] However, in this tumor, immunohistochemical studies showed that the atypical cells were negative for CD30. As for SC, lesions of the lung and anterior mediastinum were absent, and spindle or giant atypical cells were not apparent histologically in the present case. IMFH is composed of xanthogranulomatous inflammation with scattered atypical large cells with prominent nucleoli. The present tumor lacked xanthogranulomatous inflammation, and histiocytoid cells were not so large and nucleoli were inconspicuous. IMT is composed of a variable mixture of collagen, inflammatory cells and cytologically bland spindle cells having myofibroblastic differentiation. However, in the present case, collagen and these bland spindle cells were absent. LHM is a variant of sarcomatoid malignant mesothelioma, characterized by diffuse proliferation of large, ovoid histiocyte-like and spindle cells, uniformly intermixed with a prominent lymphocytic or lymphoplasmacytic infiltrate.[3,4] But in the present case the lymphocytic or lymphoplasmacytic infiltrate was subtle.

We made a diagnosis of PSMM consisting of histiocytoid cells based on percutaneous needle biopsy specimens. The keys to accurate diagnosis were as follows: (i) recognition of serosal tumor; (ii) immunohistochemical positivity for AE1/AE3, vimentin and mesothelial markers including D2-40,[5] WT1 and HBME-1; and (iii) being aware of the varied histopathological manifestations of PSMM.

Kunimitsu Kawahara,[1] Teruaki Nagano,[1] Kaoru Matsui,[2] Toshiaki Kawai,[3] and Teruo Iwasaki[4]

Departments of [1]Pathology, [2]Thoracic Malignancy and [4]Thoracic Surgery, Osaka Prefectural Medical Center for Respiratory and Allergic Diseases, Habikino and [3]Department of Pathology, National Defense Medical College, Tokorozawa, Japan

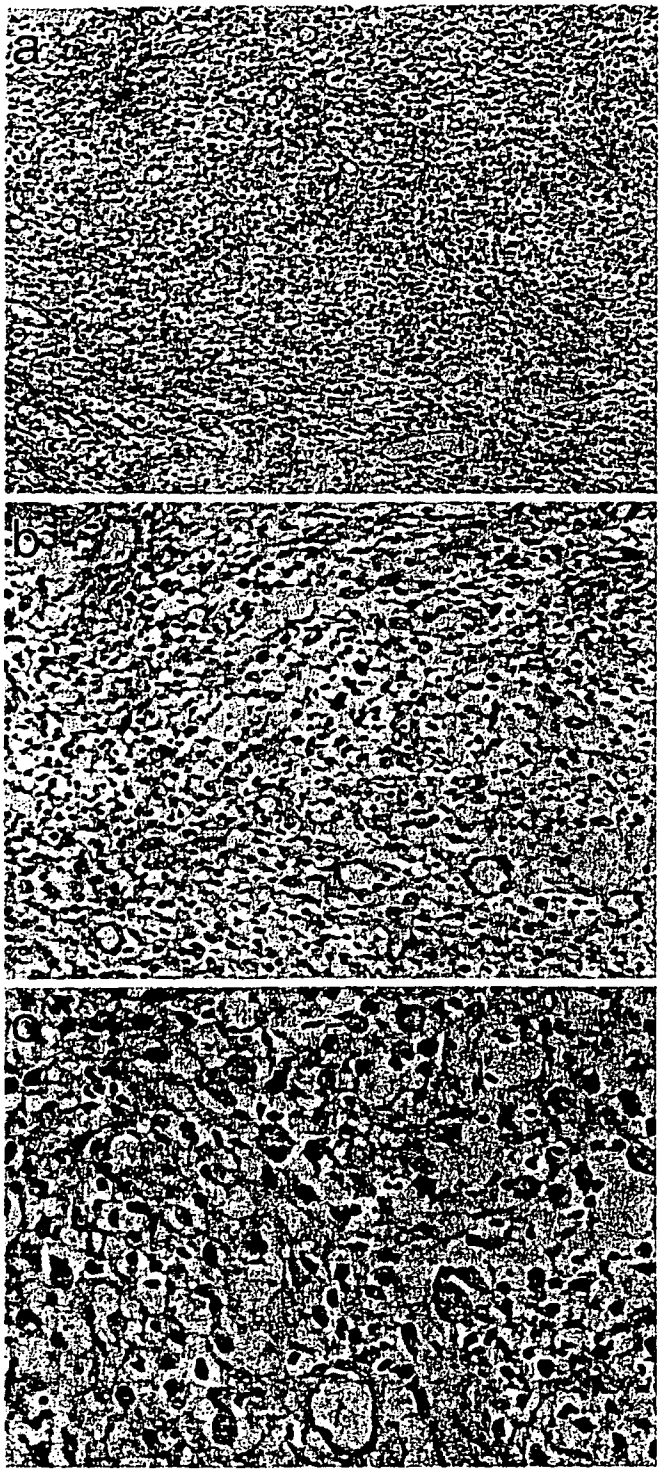

Figure 1 Microscopic view of the tumor. (**a**) Tumor cells infiltrating diffusely in a myxoid stroma. (**b**) Tumor cells mainly composed of histiocytoid cells. (**c**) The tumor cells were ovoid or polyhedral in shape with palely eosinophilic or foamy cytoplasm. Stain: HE.

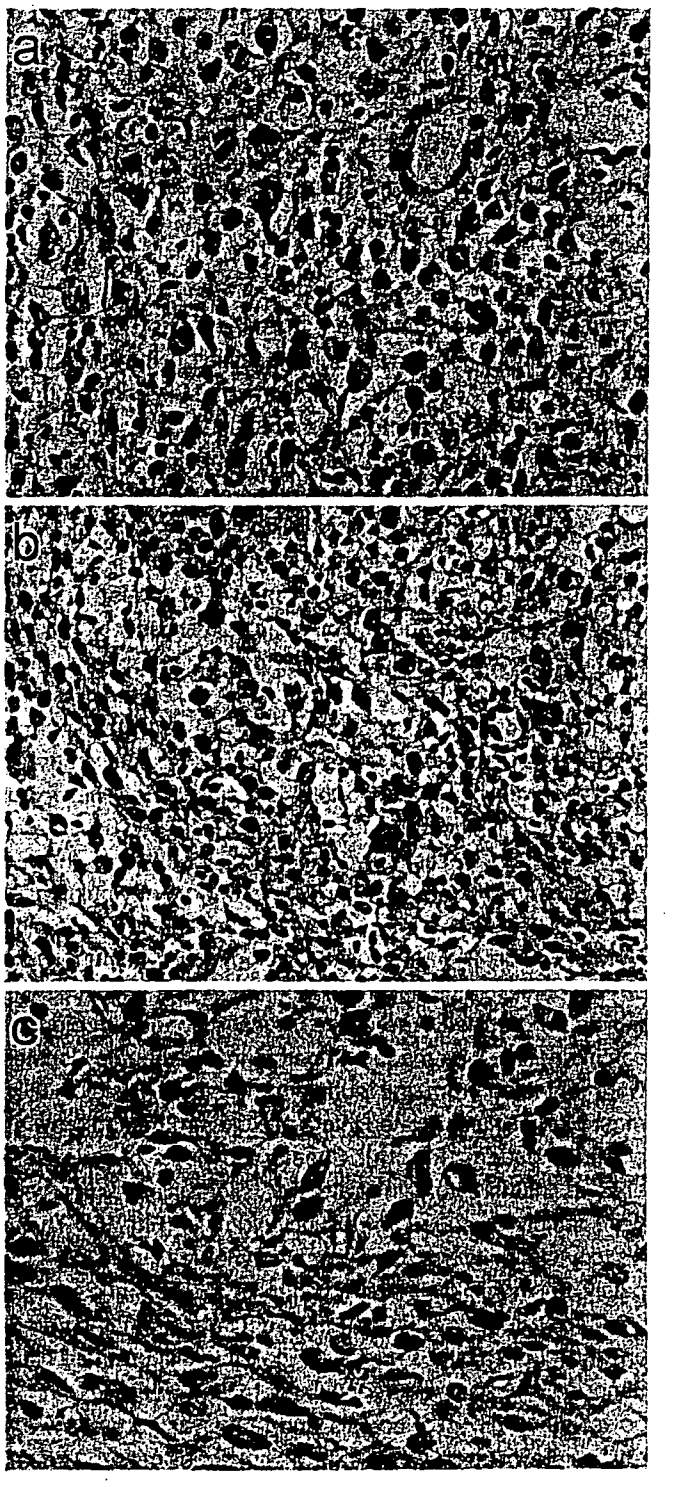

Figure 2 Immunohistochemical staining of the tumor. The histiocytoid cells had positive staining for (**a**) AE1/AE3, (**b**) D2-40 and (**c**) WT1.

REFERENCES

1 Churg A, Roggli V, Galateau-Salle F *et al.* Mesothelioma. In: Travis WD, Brambilla E, Muller-Hermelink HK, Harris CC, eds. *World Health Organization Classification of Tumors. Pathology and Genetics of Tumors of the Lung, Pleura, Thymus and Heart.* Lyon: IARC Press, 2004; 128–36.

2 Pileri S, Falini B, Delsol G *et al.* Lymphohistiocytic T-cell lymphoma (anaplastic large cell lymphoma CD30+/Ki-1+ with a high

content of reactive histiocytes). *Histopathology* 1990; **16**: 383–91.
3 Henderson DW, Attwood HD, Constance TJ, Shilkin KB, Steele RH. Lymphohistiocytoid mesothelioma: A rare lymphomatoid variant of predominantly sarcomatoid mesothelioma. *Ultrastruct Pathol* 1988; **12**: 367–84.
4 Khalidi HS, Medeiros LJ, Battifora H. Lymphohistiocytoid mesothelioma. An often misdiagnosed variant of sarcomatoid malignant mesothelioma. *Am J Clin Pathol* 2000; **113**: 649–54.
5 Chu AY, Litzky LA, Pasha TL, Acs G, Zhang PJ. Utility of D2-40, a novel mesothelial marker, in the diagnosis of malignant mesothelioma. *Mod Pathol* 2005; **18**: 105–10.

Proteomics-based identification of α-enolase as a tumor antigen in non-small cell lung cancer

Ping He,[1] Tetsuji Naka,[1,2,8] Satoshi Serada,[3] Minoru Fujimoto,[1,2] Toshio Tanaka,[1] Shoji Hashimoto,[4] Yoshihito Shima,[1] Tomoki Yamadori,[1] Hidekazu Suzuki,[5] Tomonori Hirashima,[5] Kaoru Matsui,[5] Hiroyuki Shiono,[6] Meinoshin Okumura,[6] Toshiro Nishida,[7] Isao Tachibana,[1] Naoko Norioka,[3] Shigemi Norioka[3] and Ichiro Kawase[1]

[1]Department of Molecular Medicine, Osaka University Graduate School of Medicine, 2-2 Yamadaoka, Suita, Osaka 565-0871; [2]Laboratory for Immune Signal, National Institute of Biomedical Innovation, 7-6-8 Saito-asagi, Ibaragi, Osaka 567-0085; [3]Functional Proteomics Group, Osaka University Graduate School of Frontier Biosciences, 1-3 Yamadaoka, Suita, Osaka 565-0871; [4]Division of Infection Control and Prevention, Osaka University Hospital, 2-2 Yamadaoka, Suita, Osaka 565-0871; [5]Department of Thoracic Malignancy, Osaka Prefectural Medical Center for Respiratory and Allergic Diseases, 3-7-1 Habikino, Habikino, Osaka 583-8588; [6]Department of Surgery, Division of General Thoracic Surgery, Osaka University Graduate School of Medicine, 2-2 Yamadaoka, Suita, Osaka 565-0871; [7]Department of Surgery (E1), Osaka University Graduate School of Medicine, 2-2 Yamadaoka, Suita, Osaka 565-0871, Japan

(Received December 17, 2006/Revised April 3, 2007/Accepted April 6, 2007/Online publication May 16, 2007)

Autoantibodies against tumor antigens represent one type of biomarker that may be assayed in serum for detection of cancer and monitoring of disease progression. In the present study, we used a proteomics-based approach to identify novel tumor antigens in non-small cell lung cancer (NSCLC). By combining two-dimensional electrophoresis, western blotting, mass spectrometry and enzyme-linked immunosorbent assay technology, we detected autoantibodies against α-enolase in a subset of NSCLC patients' sera. When 'Mean $OD_{\text{healthy control sera}}$ + 3 $SD_{\text{healthy control sera}}$' was used as the cut-off point, the prevalence of this autoantibody was 27.7% in patients with NSCLC (26 of 94), 1.7% in healthy control subjects (1 of 60), and not detectable in sera from 15 patients with small cell lung cancer, 18 patients with gastrointestinal cancer and nine patients with *Mycobacterium avium* complex infection of lung. Immunohistochemical staining showed that expression of α-enolase was increased in cancer tissues of NSCLC patients, and flow cytometric analysis confirmed the expression of α-enolase at the surface of cancer cells. The combined detection of autoantibodies against α-enolase, carcinoembryonic antigen and cytokeratin 19 fragment (CYFRA21-1) enhanced sensitivity for the diagnosis of NSCLC. Therefore, autoantibodies against α-enolase may constitute a promising biomarker for NSCLC. (*Cancer Sci* 2007; 98: 1234–1240)

Lung cancer is the leading cause of cancer death,[1] and NSCLC accounts for nearly 80% of lung cancer cases. There is an urgent need for a better understanding of the biological mechanisms of NSCLC as well as the identification of reliable biomarkers for its diagnosis and prognosis. To date, a number of NSCLC markers have been evaluated, including CEA, CYFRA 21-1, SCC antigen, CA125 and NSE.[2–8] Autoantibodies against several tumor antigens such as L-myc and c-myc, p53 and antineural/antinuclear antigens have also been investigated.[9–12] Recently, autoantibodies against PGP9.5, peroxiredoxin-I, annexin-I and annexin-II were identified in the sera of lung cancer patients using a proteomic approach.[13–15] However, the sensitivity and specificity of these biomarkers are not yet satisfactory and there are currently no data to support any particular method for screening for lung cancer.[16]

Autoantibodies against tumor antigens represent one type of biomarker that may be assayed in serum for detection of cancer and monitoring of disease progression. In spite of the fact that the quantity of any tumor antigen in cancer cells or in the circulation is usually very small, especially in the early stages of cancer, the body's immune response to such antigens represents a remarkable phenomenon of biological amplification of these weak signals from tumor antigens.[17] The identification of panels of tumor antigens that elicit an immune response may thus be useful for detecting potential specific biomarkers as well as for the initiation of immunotherapy against NSCLC. The aim of the present study was to identify novel candidate tumor antigens in NSCLC by means of a proteomics-based approach. One of these antigens was identified as α-enolase, and its immunogenicity was confirmed by western blotting using recombinant protein. The results obtained with enzyme-linked immunosorbent assay (ELISA) demonstrated that when 'Mean $OD_{\text{healthy control sera}}$ + 3 $SD_{\text{healthy control sera}}$' was used as the cut-off point, a humoral immune response directed against α-enolase occurred in 27.7% of NSCLC patients, but in only 1.7% of healthy control subjects. Immunohistochemical staining showed that α-enolase was overexpressed in cancer tissues of NSCLC patients. The combined detection of autoantibodies against α-enolase, CEA and CYFRA 21-1 enhanced sensitivity for NSCLC diagnosis. Therefore, autoantibodies against α-enolase may constitute a promising biomarker for NSCLC.

Materials and Methods

Subjects. Sera and tumor tissue were obtained at the time of diagnosis after informed consent had been given by the subjects. The experimental protocol was approved by the ethics committee of Osaka University. Sera from 94 patients with NSCLC, 15 patients with SCLC, 18 patients with gastrointestinal cancer (10 patients with gastric cancer, 8 patients with colon cancer) and nine patients with MAC were analyzed. In terms of TNM stages, the NSCLC patients comprised 17 cases of stage I, 14 cases of stage II, 34 cases of stage III and 29 cases of stage IV. The histological distribution of NSCLC was 73 adenocarcinoma cases and 21 SCC cases. Clinical data for the serum tumor marker CEA and CYFRA 21-1 were also collected for investigation. Sera from 60 asymptomatic healthy subjects, whose average age and sex were comparable to those of the NSCLC patient group, were used as controls.

1-DE and 2-DE. Proteins were extracted from NSCLC tumor tissues using the Complete Mammalian Proteome Extraction Kit (Calbiochem, Darmstadt, Germany). For 1-DE, extracted proteins

[8]To whom correspondence should be addressed. E-mail: tnaka@nibio.go.jp

Abbreviations: 1-DE, one-dimensional electrophoresis; 2-DE, two-dimensional electrophoresis; a.a., amino acids; CA, cancer antigen; CBB, Coomassie brilliant blue; CEA, carcinoembryonic antigen; CYFRA21-1, cytokeratin 19 fragment; ELISA, enzyme-linked immunosorbent assay; HRP, horseradish peroxidase; IEF, isoelectric focusing; IHC, immunohistochemical; LC, liquid chromotography; MAC, Mycobacterium avium complex; MALDI-TOF, matrix-assisted laser desorption–ionization time-of-flight; MS, mass spectrometry; NSCLC, non-small cell lung cancer; NSE, neuronspecific enolase; OD, optical density; PCR, polymerase chain reaction; PMF, peptide mass fingerprinting; PVDF, polyvinylidene difluoride; SCC, squamous cell carcinoma; SCLC, small cell lung cancer; TNM, tumour–node–metastasis.

doi: 10.1111/j.1349-7006.2007.00509.x

were resolved by using 10% Bis-Tris Criterion XT Precast gels (Bio-Rad Laboratories, Hercules, CA, USA), transferred to PVDF membranes or stained with CBB. For 2-DE, IEF was carried out using the PROTEAN IEF cell (Bio-Rad Laboratories) according to the manufacturer's instructions. Extracted proteins were reconstituted in a rehydration buffer (7 M urea, 2 M thiourea, 4% CHAPS, 2 mM tributyl phosphine (TBP), 0.0002% bromophenol blue (BPB), 0.2% bio-lyte ampholyte 3-10) and applied to ReadyStrip IPG strips (11 cm, pH 3–10). IEF was run for 45 000 Vh, and 2-DE was carried out using 10% Bis-Tris Criterion XT Precast gels. The gels were then stained with the Silver Stain MS Kit (Wako Pure Chemical Industries, Osaka, Japan) or used for protein transfer to PVDF membranes.

Western blotting. After blocking with 5% skim milk, the PVDF membranes were incubated with serum at a 1:100 dilution or rabbit anti-enolase antibody (Santa Cruz Biotechnology, Santa Cruz, CA, USA) at a 1:1500 dilution. The membranes were then incubated with sheep anti-human IgG or donkey anti-rabbit IgG (Amersham Biosciences UK, Buckinghamshire, UK). Membranes incubated with sheep anti-human IgG only were used as negative controls. Finally, the signals were visualized with an enhanced chemiluminescence reaction system (Perkin Elmer Life Sciences, Boston, MA, USA).

Identification of protein bands or spots. Protein bands on gels stained with CBB or protein spots on gels stained with silver, which corresponded to positive bands or spots on western blot membranes, were excised from the gel and digested with trypsin (Promega, Madison, WI, USA) according to published procedures.[18] For protein bands, the LC-MS/MS analysis was carried out using an LCQ ion trap mass spectrometer (ThermoElectron, San Jose, CA, USA) coupled on-line with Magic 2002 capillary high-performance liquid chromatography (Michrom BioResources, Auburn, CA, USA). For protein spots, all PMF spectra were obtained by using an ultraflex TOF/TOF MALDI-TOF mass spectrometer (Bruker Daltonics, Bremen, Germany). MS/MS or PMF data were then searched with Mascot software (Matrix Science, London, UK) against the NCBInr or swiss-prot databases. Protein database searching was carried out with following parameters for PMF: *Homo sapiens*, maximum of one missed, cleavage by trypsin, monoisotopic mass value, charge state of 1+, allowing a mass tolerance of 100 p.p.m., and carbamidomethyl modification of cysteine.

Preparation of recombinant protein. To prepare recombinant proteins, the human full-length α-enolase complementary DNA (1–434 a.a.) was amplified by PCR from the Hep3B cell line cDNA library using the primers: sense 5′-GTGGCTAGAAGTTCACCATG-3′, antisense 5′-TTACTTGGCCAAGGGGTTTC-3′. To map the autoepitope on α-enolase, three cDNA fragments that encode C-terminal deletion mutant proteins (α-Eno1, α-Eno2, α-Eno3) were similarly amplified. The nucleotide sequences of the primers for PCR were: α-Eno1 (1–334 a.a.) sense 5′-TGTCTATTCTCAAGATCCATGCC-3′, antisense 5′-TTACTCGTTCACGGCCTTGGC-3′; α-Eno2 (1–234 a.a.), sense 5′-TGTCTATTCTCAAGATCCATGCC-3′, antisense 5′-TTAAGCTTTCCCAATAGCAGTC-3′; and α-Eno3 (1–134 a.a.) sense 5′-TGTCTATTCTCAAGATCCATGCC-3′, antisense 5′-TTAGATGTGGCGGTACAGGGG-3′. These cDNA fragments were then subcloned into the pET-28a(+) vector (Novagen, Madison, WI, USA), resulting in expression of α-enolase or its fragments with a 6 × His tag. Recombinant proteins were produced in *Escherischia coli* BL21-CodonPlus (DE3)-RIL cells (Stratagene, La Jolla, CA, USA) and purified by affinity chromatography using Ni-NTA resin (QIAGEN, Tokyo, Japan). Recombinant human full-length or C-terminal deletion mutant α-enolase, rabbit β-enolase (Sigma, St Louis, MO, USA) and human γ-enolase (Calbiochem) were subjected to sodium dodecylsulfate–polyacrylamide gel electrophoresis, using a 4–20% precast gel, then stained with CBB or transferred to PVDF membrane and probed with anti-enolase antibody, anti-6 × His monoclonal antibody or sera as described above.

Flow cytometry. Human lung adenocarcinoma cell line A549 was maintained in RPMI-1640 medium supplemented with 10% heat-inactivated fetal bovine serum, 100 U/mL penicillin and 100 μg/mL streptomycin. Cells (10^6) were incubated with rabbit anti-enolase antibody at a 1:100 dilution and labeled with fluorescein isothiocyanate-conjugated goat anti-rabbit immunoglobulin (BD Biosciences, San Jose, CA, USA). Normal rabbit IgG was used as a control. Stained cells were analyzed using a FACS Canto cytometer (Becton-Dickinson, Mountain View, CA, USA) and the results were analyzed using FlowJo software (Tree Star, Stanford, CA, USA).

ELISA. To assess the potential of these autoantibodies as a diagnostic marker, their frequencies in the sera were determined by means of ELISA using recombinant human full-length α-enolase protein. The ELISA was carried out as published elsewhere, with modifications.[19] Briefly, each well of a Microtiter plate (MaxiSorp; Nunc A/S, Roskilde, Denmark) was coated with 1 μg of recombinant human full-length α-enolase. After blocking with 1% bovine serum albumin, all wells were incubated with human serum at a 1:500 dilution at room temperature for 1 h. To reduce the background level originating from the non-specific reactivity of sera with bacterial proteins, the sera were diluted and incubated with 100 μg/mL *E. coli* BL21-CodonPlus (DE3)-RIL cell lysate for 2 h at room temperature before incubation with coated recombinant human α-enolase. The antigen–antibody complexes were detected with 1:5000-diluted HRP-conjugate sheep anti-human IgG with TMB (Dako, Carpinteria, CA, USA) as the substrate. OD was read at 450 nm. The antibody titer was expressed by using arbitrary binding units calculated according to the formula:

$$\text{binding units of sample} = (OD_{\text{sample}}/[\text{Mean } OD_{\text{healthy control sera}} + 3\ SD_{\text{healthy control sera}}]) \times 100.$$

Based on this formula, 100 binding units was used as the cut-off point.

IHC staining. After deparaffinization, tissue sections were treated with 100% cold methanol containing freshly prepared 0.3% hydrogen peroxide for 30 min, blocked in 10% normal goat serum for 20 min and incubated with rabbit anti-enolase antibody (Santa Cruz Biotechnology) at a 1:250 dilution overnight. Incubation of parallel sections omitting the first antibody was done to generate negative controls. Staining of sections was completed with a biotin-conjugated secondary antibody, HRP-conjugated streptavidin and diaminobenzidine.

Statistical analysis. Significant differences between groups were assessed with the χ^2-test and Fisher's exact test. $P < 0.05$ was considered significant.

Results

Detection of autoantigens associated with NSCLC by 1-DE western blotting and LC-MS/MS. In order to screen for autoantibodies against cancer cells in patients with NSCLC, proteins extracted from a given patient's tumor tissue were subjected to 1-DE, transferred to membranes, and incubated with sera from the same patient or from healthy control subjects. Membranes incubated with only the secondary antibody were used as negative controls. An approximately 47-kDa band was recognized only by a subset of NSCLC patient sera, whereas no such reaction was observed with healthy control sera or negative controls (Fig. 1a). To identify this 47-kDa protein, the corresponding band on the gel stained with CBB was digested and analyzed using LC-MS/MS. The eight proteins, including α-enolase and elongation factor 1-α 1, which were identified by database searching through Mascot software, are listed in Table 1. Many of these proteins

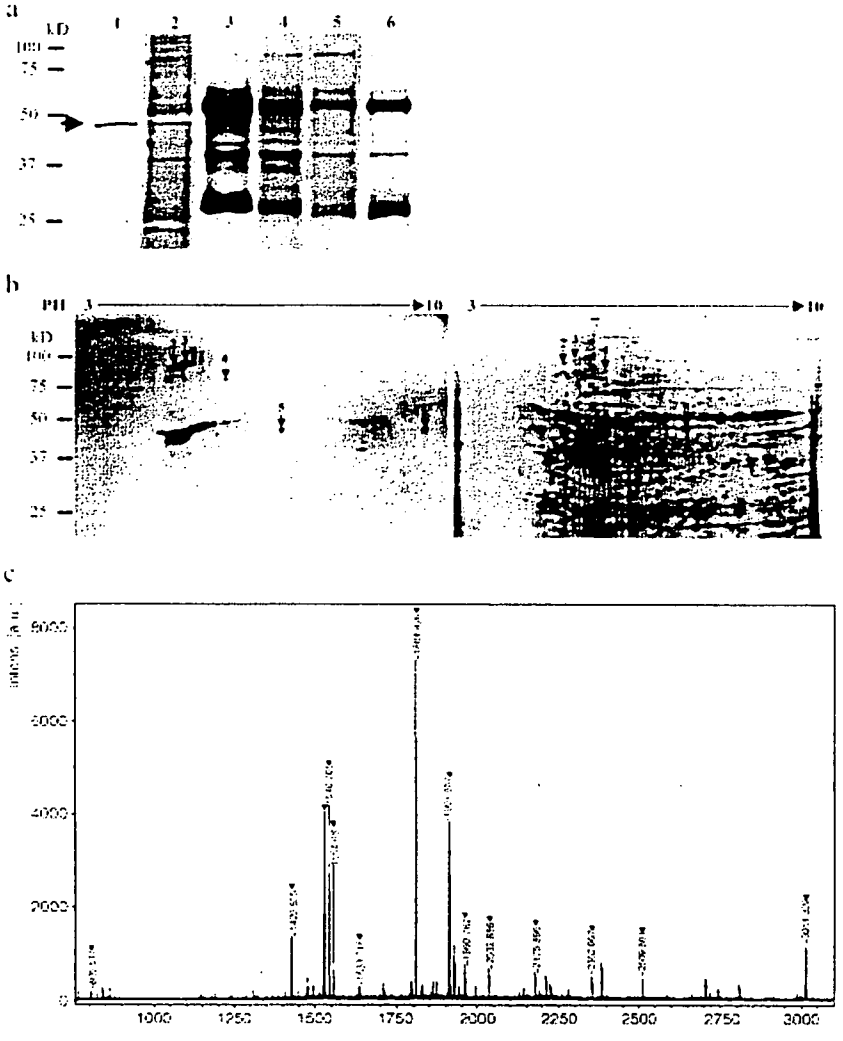

Fig. 1. (a) Screening by means of one-dimensional electrophoresis (1-DE) western blotting analysis for autoantigen associated with non-small cell lung cancer (NSCLC). Lane 1: ~47-kDa positive band (arrow), which was recognized by anti-enolase antibodies. Lanes 2, 3: 47-kDa positive band, which was recognized by NSCLC sera. Lane 4: no 47-kDa positive band was observed in a negative NSCLC case. Lane 5: no positive reaction was observed with healthy control sera. Lane 6: no positive reaction was observed in negative controls. (b) Detection by means of two-dimensional electrophoresis (2-DE) western blotting analysis of autoantigen associated with NSCLC. Left panel: Representative 2-DE western blotting analysis. Right panel: corresponding 2-DE silver-stained image. Protein spots recognized only by NSCLC sera are marked with arrows and numbers. (c) Peptide mass fingerprinting spectra of positive spot 5. For spot 5, 14 peptide masses were matched with human α-enolase by executing an NCBInr database search, yielding 52% protein sequence coverage. The matched mass peaks are marked with arrow heads.

Table 1. Mascot search results of the liquid chromatography-mass spectrometry/mass spectrometry (LC-MS/MS) data

Protein name	Swiss Prot Accession number	Molecular weight (Da)	pI	Score*	Peptide matched	Protein coverage (%)
Elongation factor 1-α 1	P68104	50 451	9.10	123	4	7
Cytokeratin 17	Q04695	48 230	4.97	271	13	25
α-Enolase	P06733	47 037	6.99	96	3	5
Elongation factor Tu	P49411	49 852	7.26	56	1	3
α-1-acid glycoprotein 1 precursor	P02763	23 725	4.93	160	4	18
Vimentin	P08670	53 545	5.06	115	5	9
Albumin precursor	P02768	71 317	5.92	106	4	6
Actin-like protein 3	P61158	47 797	5.61	46	2	7

*Scores > 39 indicate identity or extensive homology ($P < 0.05$). To identify the 47-kDa protein recognized only by non-small cell lung cancer patient sera, the corresponding band stained with Coomassie brilliant blue was digested and analyzed by LC-MS/MS. The eight proteins identified are listed.

are of similar molecular weight and one of them may be the autoantigen associated with NSCLC. We used western blotting with rabbit anti-enolase antibodies to confirm that the expression of α-enolase occurred at the same position as that of the 47-kDa positive band (Fig. 1a).

Autoantibodies against α-enolase present in NSCLC patient sera. To characterize autoantibodies in NSCLC sera, proteins extracted from a given patient's tumor tissue were separated by 2-DE, transferred to membranes, and incubated with sera from the same patient or from healthy control subjects. Compared with the sera of healthy control subjects, 2-DE western blotting with NSCLC patient sera showed five positive protein spots (Fig. 1b, left panel), including one spot (spot 5) that also had a molecular weight of approximately 47 kDa and a pI value of

doi: 10.1111/j.1349-7006.2007.00509.x

Table 2. Mascot search results of matrix-assisted laser desorption–ionization time-of-flight (MALDI-TOF) data

Spot no.	Protein name	Sequence coverage (%)	Molecular weight (Da)	pI
1	Chain D, myeloperoxidase	22	53 806	9.43
2	Tumor rejection antigen-1 (gp96)	17	92 696	4.76
3	Not identified			
4	α glucosidase II α subunit	15	86 236	5.71
5	α-enolase	52	47 037	6.99

To identify the immunoreactive spots in two-dimensional electrophoresis western blotting analysis recognized by non-small cell lung cancer patient sera, corresponding silver-stained spots were digested and analyzed by MALDI-TOF/mass spectrometry. 'Spot no.' corresponds to spots marked in Fig. 1b.

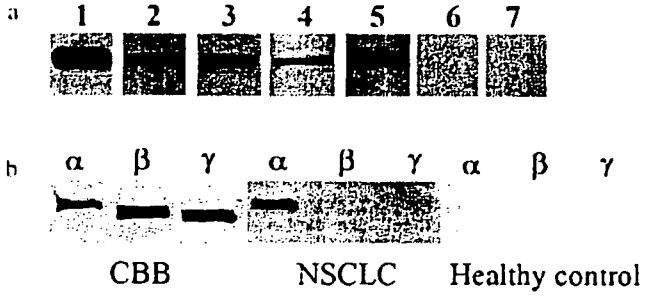

Fig. 2. (a) Western blotting analysis of recombinant human full-length α-enolase protein. Recombinant human full-length α-enolase protein was probed with rabbit anti-enolase antibodies (lane 1), with sera from non-small cell lung cancer (NSCLC) patients (lane 2–5), and with sera from healthy control subjects (lane 6–7). (b) Western blotting analysis of α, β and γ-enolase. α, β and γ-enolase protein were stained with Coomassie brilliant blue (left panel) or probed with sera from NSCLC patients (middle panel) and from healthy control subjects (right panel).

approximately 7.0. The corresponding spots on the silver-stained gel (Fig. 1b, right panel) were identified by MALDI-TOF/MS and database search. The identified proteins are summarized in Table 2. Spot 5 was recognized as α-enolase, as in the previous LC-MS/MS analysis. Its PMF spectrum is shown in Fig. 1c and the database search produced 14 peptide masses that coincided with human α-enolase, thus yielding 52% protein sequence coverage.

Next, western blotting with full-length recombinant human α-enolase protein was used to confirm and analyze the immunogenicity of α-enolase. Correct expression of the recombinant protein was verified by western blotting using rabbit anti-enolase antibodies (Fig. 2a). The recombinant proteins were then probed with sera from NSCLC patients or healthy control subjects, and positive bands were detected only in sera from the former, not from the latter (Fig. 2a). In addition, western blotting was used to determine the reactivity of NSCLC patient sera to enolase isoforms, which contain α, β and γ-enolase. The sera that were positive for autoantibodies against α-enolase reacted with neither β-enolase nor γ-enolase (Fig. 2b), whereas healthy control sera did not react with any of the enolase isoforms. This indicates the specificity of autoantibodies against α-enolase in NSCLC patient sera, and the overall results suggest that a subset of NSCLC patient sera contains autoantibodies against α-enolase.

Frequencies of autoantibodies against α-enolase in the sera were determined by means of ELISA using recombinant human full-length α-enolase protein. We tested 94 sera from patients with NSCLC, 15 from patients with SCLC, 18 from patients with gastrointestinal cancer (10 patients with gastric cancer, 8 patients with colon cancer), nine from patients with MAC infection of lung and 60 from healthy control subjects. When

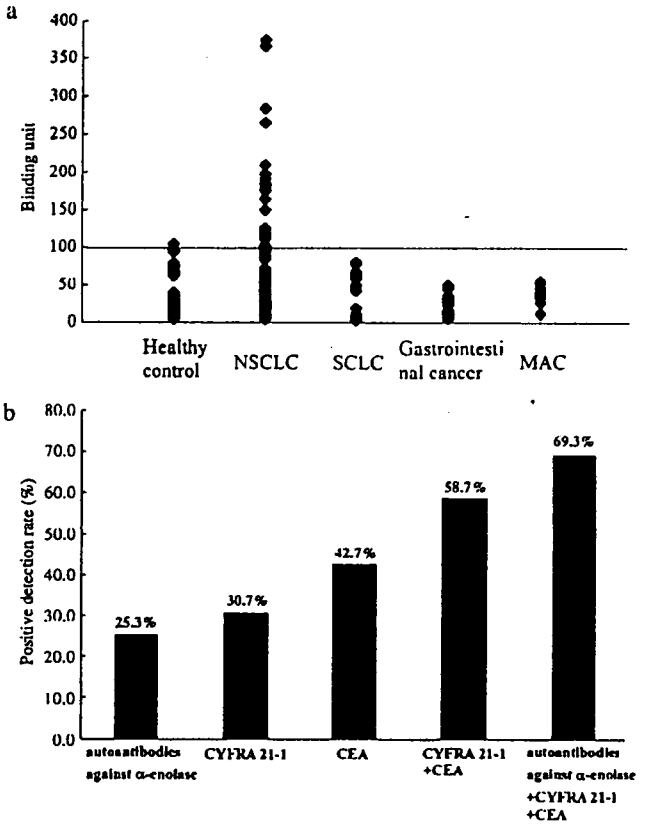

Fig. 3. (a) Prevalence of autoantibodies against α-enolase determined by enzyme-linked immunosorbent assay (ELISA). The *y*-axis denotes binding units. The solid horizontal line represents the positive cut-off limit. The prevalence of autoantibodies against α-enolase was 27.7% in patients with non-small cell lung cancer (NSCLC) (26 of 94), 1.7% in healthy control subjects (1 of 60), and not detectable in small cell lung cancer gastrointestinal cancer (10 patients with gastric cancer, 8 patients with colon cancer) and *Mycobacterium avium* complex infection of lung. (b) Positive detection rate of autoantibodies against α-enolase, cytokeratin 19 fragment (CYFRA21-1) and carcinoembryonic antigen (CEA) in NSCLC patients. Detection of CYFRA 21-1 and CEA in combination increased the positive detection rate to 58.7%. Furthermore, combined detection of autoantibodies against α-enolase, CEA and CYFRA 21-1 achieved a positive detection rate of up to 69.3%.

'Mean $OD_{\text{healthy control sera}}$ + 3 $SD_{\text{healthy control sera}}$' was used as the cut-off point, the prevalence of autoantibodies against α-enolase was 27.7% in patients with NSCLC (26 of 94), 1.7% in healthy control subjects (1 of 60), and not detectable in SCLC, gastrointestinal cancer or MAC infection of lung (Fig. 3a). These results

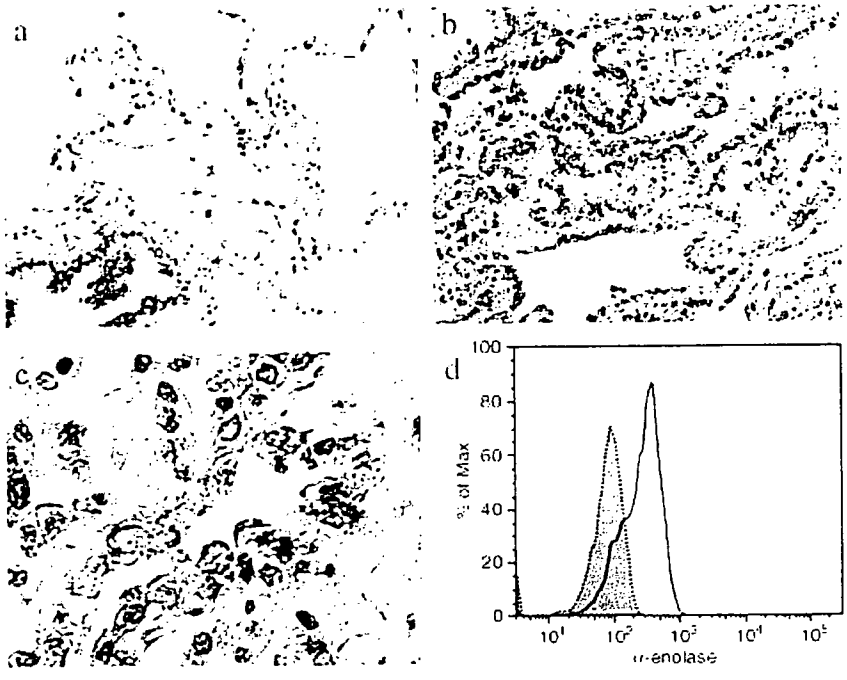

Fig. 4. Immunohistochemical and flow cytometric analysis of α-enolase. (a) Normal lung tissue (×100). (b) Lung adenocarcinoma (×100). (c) α-Enolase staining showing a mixture of cytoplasmic, and membranous immunoreactivity (×400). (d) A549 cells were stained with anti-enolase antibody, labeled with fluorescein-isothiocyanate-conjugated goat antirabbit immunoglobulin, and analyzed on a FACS Canto (open histogram). Shaded histogram indicates staining with control IgG.

showed that titers of autoantibodies against α-enolase are increased in a subset of NSCLC patients. Next, we examined the correlation between the prevalence of autoantibodies against α-enolase and clinicopathological features in NSCLC patients. Positive reactivity was detected in 21 of the 73 sera from adenocarcinoma patients (28.8%) and in five of the 21 sera from SCC patients (23.8%). There was no significant correlation between the occurrence of autoantibodies against α-enolase and pathological types ($P = 0.654$). In addition, there was a tendency for autoantibodies against α-enolase to be more prevalent in patients with advanced NSCLC cases (stage III/IV, 33.3%, 21 of 63) than in stage I/II cases (16.1%, 5 of 31), although the results of the statistical analysis suggest that the prevalence has no significant correlation with disease stage ($P = 0.08$). We also investigated the relationship between autoantibodies against α-enolase and other tumor markers (CEA, CYFRA 21-1) that have been applied to clinical practice in NSCLC patients. In a total of 94 NSCLC patients, clinical data of both CEA and CYFRA 21-1 were available for 75 patients. In these patients, 25.3% (19/75) were positive for autoantibodies against α-enolase, 42.7% (32/75) were positive for CEA, and 30.7% (23/75) were positive for CYFRA 21-1. The occurrence of autoantibodies against α-enolase didn't show a significant correlation with CEA ($P = 0.63$) or with CYFRA 21-1($P = 0.92$). Detection of CYFRA 21-1 and CEA in combination increased the positive detection rate to 58.7% (44/75). Furthermore, positive detection rate was enhanced up to 69.3% (52/75) when combined detection of autoantibodies against α-enolase, CEA and CYFRA 21-1 was used (Fig. 3b).

IHC and flow cytometric analysis of α-enolase. We used IHC staining to compare α-enolase expression in non-malignant and malignant lung tissues from 20 NSCLC patients, including 10 patients with autoantibodies against α-enolase and 10 patients without autoantibodies against α-enolase. The staining results showed that expression of α-enolase was increased in malignant lung tissue of NSCLC patients (Fig. 4a–c). Additionally, IHC staining showed not only cytoplasmic but also membranous immunoreactivity in cancer cells (Fig. 4c). Flow cytometric analysis of human lung adenocarcinoma cell line A549 also confirmed the expression of α-enolase at the surface of lung cancer cells (Fig. 4d).

Epitopes located at the N-terminal region (1–134 a.a.) of α-enolase that are recognized by autoantibodies. To locate the serological epitopes of α-enolase, full-length and C-terminal deletion mutant proteins (α-Eno1, α-Eno2, α-Eno3) were prepared. The full-length α-enolase (1–434 a.a.), α-Eno1 (1–334 a.a.), α-Eno2 (1–234 a.a.) and α-Eno3 (1–134 a.a.) recombinant proteins were clearly shown by an anti-6 × His antibody or stained with CBB, which verified their expression (Fig. 5). A commercially available rabbit anti-enolase antibody reacted only with the full-length α-enolase, α-Eno1 and α-Eno2 recombinant proteins (Fig. 5). However, sera from NSCLC patients who showed the presence of autoantibodies against α-enolase reacted with the α-Eno1, α-Eno2, and α-Eno3 recombinant proteins (Fig. 5), indicating that in NSCLC patients at least the N-terminal region of α-enolase contains epitopes.

Discussion

In the present study we used a proteomics-based screen test to identify proteins such as α-enolase and gp96 that may elicit a humoral immune response in NSCLC patients. We then confirmed that some NSCLC patients' sera contained autoantibodies against α-enolase by means of western blotting using recombinant protein. Furthermore, the results obtained with ELISA demonstrated that when '$\text{Mean OD}_{\text{healthy control sera}} + 3\ \text{SD}_{\text{healthy control sera}}$' was used as the cut-off point, the humoral immune response directed against α-enolase occurred in 27.7% of NSCLC patients, but in only 1.7% of healthy control subjects. α-enolase is an isoenzyme of enolase, a key protein that catalyzes the conversion of 2-phosphoglycerate to phosphoenolpyruvate, which is the second of the two high-energy intermediates that generate ATP in glycolysis.[20] Three isoforms of enolase have been identified and are known as α, β and γ-enolase. α-enolase is present in most tissues and is predominant in early embryonic tissue, β-enolase is expressed in muscle tissue, and γ-enolase, also known as NSE, is found only in neuronal tissues.

Autoantibody responses to tumors are generally thought to be elicited in three ways. These are overexpression of specific proteins, especially on the cell surface, gene mutation or post-translational modification of proteins, which shows new epitopes

doi: 10.1111/j.1349-7006.2007.00509.x

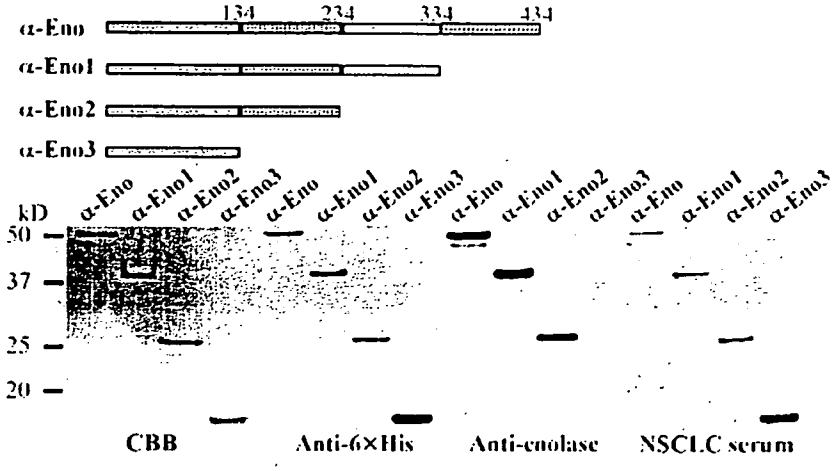

Fig. 5. Upper panel: preparation of recombinant human full-length α-enolase protein: α-Eno (1–434 a.a.), C-terminal deletion mutant α-enolase proteins: α-Eno1 (1–334 a.a.), α-Eno2 (1–234 a.a.) and α-Eno3 (1–134 a.a.). Lower panel: recombinant proteins were stained with Coomassie brilliant blue or probed with anti-6 x His antibody, anti-enolase antibody or non-small cell lung cancer sera.

as immunogens, and other types of protein processing in tumor tissue.[21] In the present study we used normal recombinant proteins to confirm the immunogenicity of α-enolase in NSCLC patients. In addition, although a past study reported that expression of α-enolase was downregulated in NSCLC tissues,[22] IHC staining used in our study showed that α-enolase expression is commonly increased in malignant lung tissue from NSCLC patients compared to the expression in non-malignant lung tissue, which is consistent with other previous reports.[23–27] Interestingly, IHC staining also showed not only cytoplasmic but also membranous immunoreactivity. Moreover, flow cytometric analysis demonstrated expression of α-enolase on the surface of lung cancer cells. We think that enhanced expression of α-enolase on cancer-cell surface might be one reason for autoantigenicity, and might be required for induction of autoantibody responses. However, α-enolase expression alone is insufficient for autoantibody production as increased expression was also found in these patients without autoantibodies against α-enolase. Further study is necessary to investigate the detailed mechanisms involved in this autoantibody response.

It is widely accepted that the propensity for glycolysis is enhanced in cancer cells because of increased cell proliferation. In fact, α-enolase, a key enzyme in the glycolysis pathway, was found to be overexpressed in 18 cancers.[25] Furthermore, although the mechanism of its surface expression and orientation on the membrane are not yet clearly understood, it is known that the C-terminal a.a. of α-enolase, lysine, is exposed at the cell surface and is involved in binding to plasminogen, which is then activated and converted to plasmin.[28] Once plasmin is stabilized at the cell surface, it in turn induces fibrinolysis.[20] In response to the upregulation of α-enolase expression, progression of the fibrinolytic system is markedly accelerated, and the resultant increase in local fibrinolysis may contribute to cancer cell invasion and metastasis. This is consistent with our finding that there was a tendency for autoantibodies against α-enolase to be more prevalent in patients with advanced NSCLC (stage III/IV) than in stage I/II cases.

Tumor markers for NSCLC are potentially useful for both diagnostic and therapeutic practice. To date, a variety of NSCLC tumor markers have been identified and the most extensively investigated circulating protein markers include CEA, CYFRA 21-1, SCC antigen, NSE and CA125.[5] The percentages of NSCLC patients who have elevated serum protein levels of the above markers are 26%–42% for CEA, 51%–74% for CYFRA 21-1, 20%–32% for SCC, 28–32% for NSE, and 46–55% for CA125, with variations depending on histology and stage.[5–8] However, because elevated serum protein levels of these markers have been observed in tumors other than NSCLC, their sensitivity and specificity are not satisfactory and their clinical applicability is limited. Our study demonstrated that when 'Mean $OD_{\text{healthy control sera}}$ + 3 $SD_{\text{healthy control sera}}$' was used as the cut-off point, autoantibodies against α-enolase occurred in 27.7% of NSCLC patients but not in those with SCLC, gastrointestinal cancer or MAC infection of the lungs. Moreover, combined detection of autoantibodies against α-enolase, CEA and CYFRA 21-1 enhanced sensitivity for the diagnosis of NSCLC. These results suggest that using autoantibodies against α-enolase has potential as a clinical biomarker for serological screening of NSCLC. Further large-scale validation studies will be needed to determine the sensitivity, specificity and positive prognostic value of this marker in real-world screening scenarios.

Autoantibodies against α-enolase have been detected in some autoimmune diseases,[20] and Fujii *et al.* report that in Hashimoto's encephalopathy one of these autoantibodies recognizes the N-terminal region of α-enolase.[29] Because our results show this same recognition in NSCLC, further experiments are warranted to compare epitopes in α-enolase as detected in NSCLC and in autoimmune diseases to determine its utility as a biomarker for NSCLC.

Acknowledgments

We would like to thank Dr S. Nomura for extremely helpful technical instructions for immunohistochemical staining. We also thank all members of our laboratory, especially Dr T. Hirano and Dr A. Ogata for their helpful discussions and support, and Ms T. Arimoto for her secretarial assistance. This study was supported by a Grant-in-Aid from the Ministry of Education, Science and Culture, Japan and the Osaka Foundation for Promotion of Clinical Immunology, Japan.

References

1 Jemal A, Siegel R, Ward E *et al.* Cancer statistics. *CA Cancer J Clin* 2006; 56: 106–30.
2 Stieber P, Aronsson AC, Bialk P *et al.* Tumor markers in lung cancer: EGTM recommendations. *Anticancer Res* 1999; 19: 2817–19.
3 Sidransky D. Emerging molecular markers of cancer. *Nat Rev Cancer* 2002; 2: 210–19.
4 Rastel D, Ramaioli A, Cornillie F, Thirion B. CYFRA 21-1, a sensitive and specific new tumor marker for squamous cell lung cancer. *Eur J Cancer* 1994; 30A: 601–6.
5 Trape J, Buxo J, Perez de Olaguer J, Vidal C. Tumor markers as prognostic